

## Ring Current Model and Anisotropic Magnetic Response of Cyclopropane

Raphaël Carion and Benoît Champagne

*Laboratoire de Chimie Théorique, Unité de Chimie Physique Théorique et Structurale, Facultés Universitaires Notre-Dame de la Paix, rue de Bruxelles, 61, B-5000 Namur, Belgium*

Guglielmo Monaco\* and Riccardo Zanasi

*Dipartimento di Chimica dell'Università degli Studi di Salerno, via Ponte don Melillo, 84084 Fisciano (SA), Italy*

Stefano Pelloni\* and Paolo Lazzeretti

*Dipartimento di Chimica dell'Università degli Studi di Modena, via Campi 183, 41100 Modena, Italy*

Received April 1, 2010

**Abstract:** Three-dimensional models of the quantum mechanical current density, induced in the electron cloud of the cyclopropane molecule by a uniform magnetic field applied either along the  $C_3$  or the  $C_2$  symmetry axes (indicated by  $B_{\parallel}$  and  $B_{\perp}$ , respectively), have been constructed via extended calculations. These models of near Hartree–Fock quality, previously shown to provide a good agreement between computed and observed values of magnetic tensors, have been used to interpret the magnitude of the diagonal components of susceptibility ( $\chi$ ), nuclear shielding of carbon ( $\sigma^C$ ) and hydrogen ( $\sigma^H$ ), and shielding at the center of mass ( $\sigma^{CM}$ ). The source of the exceptionally large in-plane component  $\sigma_{\perp}^{CM}$ , dominating the anomalous average  $\sigma_{av}^{CM}$ , is shown to be a strong delocalized current flowing around the methylene moieties and the noncyclic  $\text{CH}_2\text{—CH}_2$  fragment. The total current strength for a magnetic field applied in the direction of a  $C_2$  symmetry axis is 15.7 nA/T, approximately 1.5 times larger than that calculated for  $B_{\parallel}$ . The largest component of the susceptibility is instead the out-of-plane  $\chi_{\parallel}$ , which depends on the intensity of the  $\sigma$ -electron currents and on the entire area enclosed within the loops that they form about the  $C_3$  axis, all over its length. In a magnetic field perpendicular to the plane of the carbon atoms, both H and C nuclei sit inside diatropic whirlpools, flowing within the  $sp^3$  hybrid orbital which form the C–H bonds and extending for several bohrs above and below the  $\sigma_h$  plane. The average values and the anisotropy of carbon and proton shieldings are strongly biased by the diamagnetic shift of the out-of-plane tensor components partially determined by these vortices. The current density model of cyclopropane is revised according to these findings.

### 1. Introduction

The peculiar electronic structure of cyclopropane has prompted many investigations of its magnetic properties.<sup>1–11</sup> Indeed,

starting from the observation that in polycyclic aromatic hydrocarbons the additive rules for the average magnetizability  $\chi_{av} = (1/3)(\chi_{xx} + \chi_{yy} + \chi_{zz})$  fail, the nonadditive part of the magnetizability tensor  $\chi_{nonloc}^{nonloc}$  has been considered an indicator of electron delocalization.<sup>12</sup> Actually, as the individual components of  $\chi$  cannot be measured for mol-

\* Corresponding authors. E-mail: gmonaco@unisa.it and Stefano.Pelloni@unimore.it.

ecules in disordered phase, delocalization was more often discussed in terms of  $\chi_{av}$  and of the magnetic anisotropy  $\Delta\chi = \chi_{cc} - (1/2)(\chi_{aa} + \chi_{bb})$  in the system of  $(a, b, c)$  principal axes.<sup>12</sup>

With the advent of NMR spectroscopy, the most used delocalization probe in polycyclics became the chemical shift  $\delta^I = \sigma_{av}^{ref} - \sigma_{av}^I$  with respect to a reference compound, where  $\sigma_{av}^I = (1/3)(\sigma_{xx}^I + \sigma_{yy}^I + \sigma_{zz}^I)$  is the average magnetic shielding of nucleus  $I$ . Thanks to the development of powerful ab initio codes, accurate theoretical values of nuclear magnetic shielding and chemical shift are easily available, and the negative of the chemical shift of a ghost atom placed in a suitably defined “ring center”, referred to as nucleus independent chemical shift (NICS), has also been widely used as a measure of magnetotropicity in connection with local, or nonlocal, effects.<sup>13,14</sup> Arguably, if the largest component  $\beta_{cc}$  of a magnetic tensor  $\beta \equiv \chi, \sigma^I$  has a dominant nonlocal component, one expects  $3\beta_{av}^{nonloc} \approx \beta_{cc}^{nonloc} \approx \Delta\beta^{nonloc}$ . For molecules satisfying this condition, isotropic values and anisotropies should lead to analogous conclusions concerning the amount of electron delocalization on the magnetic criterion.

In 1952 the large  $\chi_{av}$  of cyclopropane was first interpreted in terms of a ring current model (RCM),<sup>1</sup> widely discussed by other authors.<sup>3,6–9,11</sup> RCMs have also been examined to rationalize the upfield proton chemical shifts of cyclopropane and its derivatives.<sup>2,4</sup>

According to the Biot–Savart law (BSL), the  $\pi$ -ring current induced by an external magnetic field  $B_z$  at right angles to the plane of benzene reinforces the applied field at the site of the protons, which lie beyond the ring current loop, thus causing a paramagnetic shift of the out-of-plane component  $\sigma_{zz}^H$  of the proton shielding. On the other hand, a ring current would diminish the applied  $B_z$  at the protons of cyclopropane, which lie inside the circuit, and thus increases  $\sigma_{zz}^H$ .<sup>2–4,15</sup>

A “ring current involving cyclic  $\sigma$ -electron delocalization among the three carbon atoms” is explicitly referred to by Dale Poulter et al.,<sup>7</sup> claiming that it would qualitatively explain the anisotropy of a cyclopropyl group discussed by several workers.<sup>2,16–18</sup> The model chosen by Dale Poulter et al. “considers the effect of electrons precessing in a circle which circumscribes the ring”, with radius 0.88 Å.<sup>7</sup> The interpretation of cyclopropane magnetic response in term of ring currents was strongly advocated by Dewar,<sup>15</sup> who proposed the much discussed<sup>19</sup> and still debated concept of  $\sigma$ -aromaticity.<sup>20</sup>

Benson and Flygare<sup>5</sup> found it surprising that the experimental value of  $\chi_{av} = -39.2 \times 10^{-6}$  erg G<sup>-2</sup> mol<sup>-1</sup> in cyclopropane is considerably larger than the corresponding value  $-28.6 \times 10^{-6}$  in cyclopropene, whereas the estimated  $\Delta\chi = -10.0 \times 10^{-6}$  erg G<sup>-2</sup> mol<sup>-1</sup> in cyclopropane is significantly smaller than  $\Delta\chi = -17.0 \pm 0.5 \times 10^{-6}$  in cyclopropene.<sup>5</sup> Therefore,  $\chi_{av}$  and  $\Delta\chi$  would seem to yield opposite orders for the amount of delocalization in these molecules.

Moreover, the constitutive corrections for rings,  $-3.2$  and  $-4.1$  ppm erg G<sup>-2</sup> mol<sup>-1</sup> estimated by these authors for the cyclopropane and cyclopropene, respectively,<sup>5</sup> are  $\approx 8.2\%$

and  $\approx 14\%$  of the experimental average susceptibility. From the atomic Pascal terms  $\chi_C = -6.00$  and  $\chi_H = -2.93$ , recently reported by Bain and Berry,<sup>21</sup> one obtains for cyclopropane  $\chi_{av}^{nonloc} = -39.2 - 3 \times (-6.00) - 6 \times (-2.93) = -3.6$  ppm erg G<sup>-2</sup> mol<sup>-1</sup>, quite close to the Benson and Flygare constitutive correction for rings.<sup>5</sup> From the experimental anisotropy of cyclopropane<sup>10</sup>  $\Delta\chi = -11.6$  ppm erg G<sup>-2</sup> mol<sup>-1</sup>, assuming the contribution  $\Delta\chi^{loc} = 1.6 \pm 0.8$  for an sp<sup>3</sup> carbon,<sup>22,23</sup> one obtains  $\Delta\chi^{nonloc} = -16.4$  ppm erg G<sup>-2</sup> mol<sup>-1</sup>. Therefore, in cyclopropane  $3\chi_{av}^{nonloc}$  differs from  $\Delta\chi^{nonloc}$  by 5.6 cgs ppm units, an amount well above experimental errors, which could be interpreted in terms of electron delocalization enhancing  $\chi_{||}$  but also affecting the in-plane component  $\chi_{\perp}$ .

The nonlocal contributions to the out- and in-plane components of the susceptibility tensor of cyclopropane, in ppm erg G<sup>-2</sup> mol<sup>-1</sup>, are easily evaluated from these data:

$$\chi_{||}^{nonloc} = \chi_{av}^{nonloc} + \frac{2}{3}\Delta\chi^{nonloc} = -14.5$$

$$\chi_{\perp}^{nonloc} = \chi_{av}^{nonloc} - \frac{1}{3}\Delta\chi^{nonloc} = 1.9$$

The estimate for the latter is difficult to understand. However, it can reasonably be expected that a positive  $\chi_{\perp}^{nonloc}$  and the large value of  $\chi_{av}^{nonloc}$  are not the only anomalies in the magnetic properties of cyclopropane. The in-plane components of carbon and proton shielding may also be biased by electron delocalization. This appears even more plausible for the huge in-plane shielding recently evaluated for a probe in the center of the cyclopropane ring.<sup>24</sup>

A definite answer to these points can be obtained by quantum chemical calculations. In 1983 Lazzaretti and Zanasi<sup>25</sup> reported the first ab initio model of magnetically induced current density for cyclopropane in a field  $\mathbf{B} = B_z \mathbf{e}_3$  orthogonal to the molecular plane, adopting a coupled Hartree–Fock (CHF) common origin (CO) procedure. Although that model does not provide a correct description of electron flow in either the vicinity of the carbon nuclei or about the midpoint of the C–C bonds, it showed two unexpected important features: (i) a central paratropic vortex and (ii) three local diatropic vortices circulating about the C nuclei.

As the model gave no clear evidence of a ring current, the authors attributed the large  $\sigma_{zz}^H$  value to the (upfield) diamagnetic shift caused by (ii). Subsequent ab initio calculations have unambiguously documented a delocalized current,<sup>26,24,27</sup> although its contribution to the magnetic properties of cyclopropane has not yet been quantified.

An RCM of cyclopropane providing an interpretation of its seemingly anomalous magnetic susceptibility, reported by Bader and Keith,<sup>26</sup> is reviewed in Section 1 of the Supporting Information. A more recent model proposed by Fowler, Baker, and Lillington (FBL),<sup>19</sup> consistent with the literature attribution of  $\sigma$ -aromaticity to C<sub>3</sub>H<sub>6</sub>,<sup>11,28,29,15,30–32</sup> is critically revised by methods outlined in Section 4, where correct criteria for vortex–saddle merging are outlined, see also Section 2 of the Supporting Information.

Recent calculations were reported by Fliegl et al., who concluded that ring currents in C<sub>3</sub>H<sub>6</sub> are not negligible because the total current strength (evaluated by numerical integration of the net current  $\mathbf{J}^B$  over a half-plane through the midpoint of a C–C bond and normal to it) is 10.0 nA/T, which is only 1.8 nA/T smaller than for benzene.<sup>27</sup> These authors claim that the strongest diatropic current flow appears in the molecular plane for both cyclopropane and benzene molecules.<sup>33</sup> Accordingly, allowing for the ring-current criterion of aromaticity, cyclopropane would be almost as aromatic as benzene, even though it is fully saturated.<sup>27</sup> The results of Fliegl et al.<sup>27</sup> are discussed in Section 6.

Allowing for the present state of affairs, this paper is primarily meant to complete the  $\mathbf{J}^B$  current density model of a previous article<sup>24</sup> at the Hartree–Fock level by (i) investigating the main features of the  $\mathbf{J}^B$  vector field for a magnetic field  $B_{\perp}$  parallel to a C<sub>2</sub> symmetry axis, (ii) analyzing the isolated critical points of  $\mathbf{J}^B$  and the related phase portraits, in terms of local effects, (iii) interpreting the difference between  $3\chi_{av}^{nonloc}$  and  $\Delta\chi^{nonloc}$ , and (iv) rationalizing the different contributions to the components of magnetic tensors. Points (i) and (iii) will at once show that the huge average NICS of cyclopropane, sometimes considered an indicator of super  $\sigma$ -aromaticity,<sup>11,28,29,34,35</sup> is instead an unreliable quantifier of magnetotropicity. These results add further evidence against the idea that NICS might really be used to assess aromaticity, the  $\sigma$ -aromatic paradigm of cyclopropane in particular.

## 2. Quantum Mechanical Current Density Models

The most interesting characteristics of a  $\mathbf{J}^B$  field are observed in the proximity of its stagnation points (SP) at which the modulus  $|\mathbf{J}^B|$  vanishes. In the neighborhood of an SP with position  $\mathbf{r}_0$  the field is described by a truncated Taylor series,

$$\begin{aligned} \mathbf{J}_\gamma^B(\mathbf{r}) = & (r_\alpha - r_{0\alpha})[\nabla_\alpha J_\gamma^B]_{\mathbf{r}=\mathbf{r}_0} + \\ & \frac{1}{2}(r_\alpha - r_{0\alpha})(r_\beta - r_{0\beta})[\nabla_\alpha \nabla_\beta J_\gamma^B]_{\mathbf{r}=\mathbf{r}_0} + \dots \quad (1) \end{aligned}$$

Within the linear approximation, an exhaustive compilation of all possible phase portraits about an SP in three-dimensional flow has been reported by Reyn,<sup>36</sup> in connection with the canonical forms of the  $3 \times 3$  Jacobian matrix  $\nabla_\alpha J_\gamma^B(\mathbf{r}_0)$ . Since the local regime depends on the eigenvalues of this matrix, SPs are classified in terms of an Euler (*rank, signature*) label.<sup>26,37–43</sup> The rank  $r$  is the number of nonvanishing eigenvalues of the Jacobian matrix and the signature  $s$  is the excess of eigenvalues with positive over negative real part. An SP is also classified in terms of its topological index  $\iota$ .<sup>44–46</sup> SPs of type (3, ±1) are called *isolated*. The corresponding phase portrait is that of *saddle node*,<sup>36</sup> if all the eigenvalues are real, or a *focus*, if two eigenvalues are complex conjugate. In the latter case, the local trajectories spiral inward or outward in the direction of the third (real) eigenvalue.

Continuous, open or closed, paths of (2,0) points are referred to as stagnation lines (SL), consisting of either *vortex*, also referred to as *center* points (index  $\iota = +1$ , two

nonvanishing complex conjugated eigenvalues), or *saddle* points (index  $\iota = -1$ , two nonvanishing real eigenvalues with the same magnitude and opposite sign). Some examples have previously been reported.<sup>24,47,26,48,41,49–53</sup>

The three-dimensional structure of a current density vector field is described by a stagnation graph (SG), which collects all isolated SPs and SLs. A (2,0) SL may branch out at (0,0) critical points. The Gomes theorem provides an index conservation constraint,  $\iota_0 = \sum_{k=1}^m \iota_k$ , for an SL with index  $\iota_0$  splitting into  $m$  new lines at a branching point.<sup>38–40,54</sup>

## 3. RCM of Cyclopropane in a Magnetic Field Perpendicular to the Plane of Carbon Nuclei

The SG for cyclopropane in a magnetic field  $B_{||}$  perpendicular to the plane of the carbon nuclei has previously been constructed employing the method of continuous transformation of the origin of the current density-diamagnetic zero (CTOCD-DZ).<sup>24</sup> As all the CTOCD variants of the current density are invariant in a translation of the origin of the gauge,<sup>56</sup> this CTOCD SG is also invariant. It illustrates in a compact way the main features of the induced current density vector field with

$$D_{3h}(C_{3h}) \equiv \{E \ 2C_3 \ 3TC_2 \ \sigma_h \ 2S_3 \ 3T\sigma_v\} \equiv \bar{6}m2$$

magnetic symmetry<sup>37</sup> (denoting time-inversion by  $T$ ) observable in Figure 1: a central paratropic vortex, i.e., a whirlpool circulating about the red SL coincident with the C<sub>3</sub> symmetry axis and parallel to  $B_{||}$ , three diatropic vortices, sustained by the carbon sp<sup>3</sup> hybrid orbitals forming the C–H bonds, and a peripheral flow of “ring currents”, with the shape of a topological torus. Each of the three green SLs passes through a C nucleus and both C and H nuclei sit inside the diatropic vortices flowing around. The SGs obtained via other calculations of increasing accuracy are reported as Supporting Information to document convergence to the Hartree–Fock limit.

A major difference from other compounds usually regarded as  $\pi$ -aromatic on the magnetic criterion<sup>48</sup> is the absence of a spatial vortex about the center of C–C bonds,<sup>26</sup> the green SL of a diatropic vortex being replaced by a blue saddle SL extending up to a pair of branching points distant more than 10 bohr from the center of the molecule.<sup>24,26</sup> Each saddle SL passes between two green isolated (3, ±1) SPs on the plane of the C nuclei, at a short distance from one another. Two more pairs of green SPs, symmetrically placed above and below the molecular plane, are also observed in the region of each C–C bond. All of them belong to a set of foci (SPs characterized by one real and two complex conjugated eigenvalues of the Jacobian matrix, see Section 2). They are connected by diatropic streamlines spiralling about them, above and below the  $\sigma_h$  symmetry plane. Asymptotic lines connect the 18 foci to the 6 saddle nodes, see Figure 2.

Since crossing of the  $\sigma_h$  plane is forbidden by magnetic symmetry,<sup>37</sup> the trajectories in the neighborhood of the foci about the midpoint of C–C bonds are *limit cycles*, which may incorrectly be interpreted as vortices in current density maps on the molecular plane, see Figure 1 of the Supporting

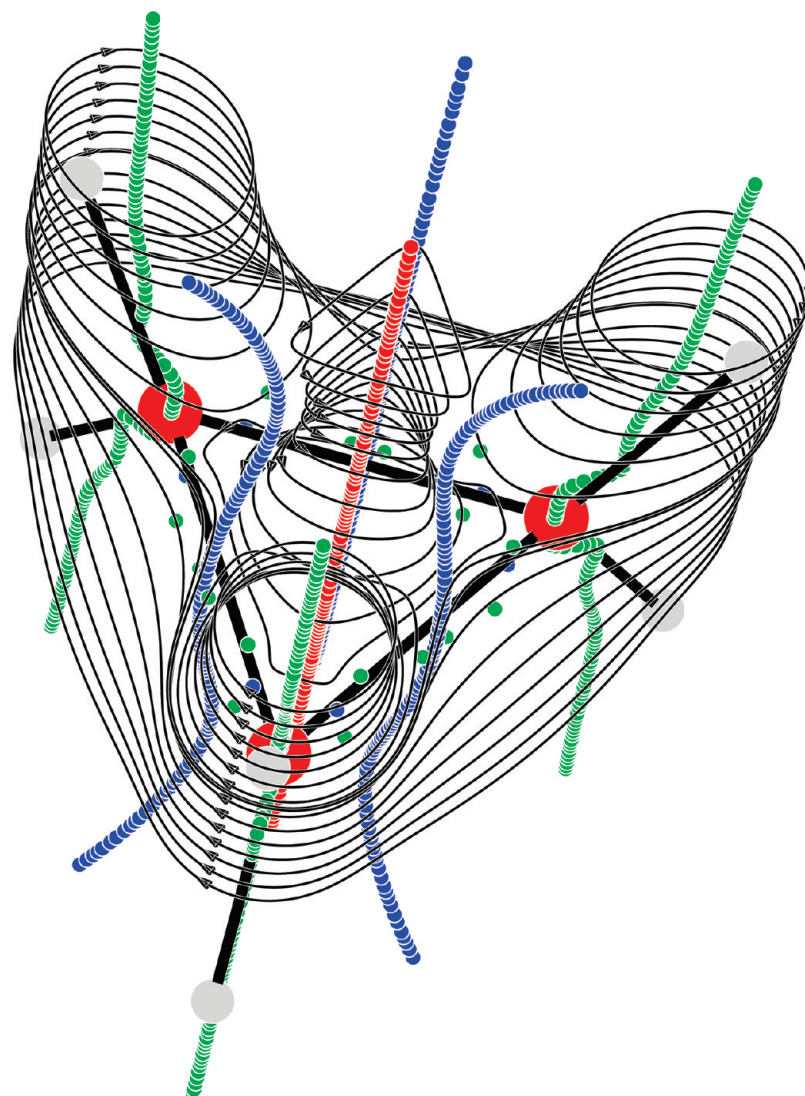


**Figure 1.** Spatial ring-current model of cyclopropane in a magnetic field perpendicular to the plane of the carbon nuclei, superimposed to the stagnation graph. A paratropic axial vortex circulates about the  $C_3$  symmetry axis. Diatropic vortices, sustained by the carbon  $sp^3$  hybrid orbitals forming the C–H bonds, are embedded within a delocalized peripheral flow (which can be described as a  $\sigma$ -ring current), having higher intensity  $|J^B|$  in a domain with the shape of a topological torus.  $|J^B|$  goes smoothly to 0 at  $\infty$ . The modulus of the current vanishes along the stagnation lines in the central region of each vortex. These continuous open lines are represented by a sequence of green (red) dots for diatropic (paratropic) regime. Saddle stagnation lines crossing the  $\sigma_h$  plane slightly outside the midpoint of a C–C bond are blue. Isolated  $(3, \pm 1)$  foci (saddle nodes) are indicated in green (blue).<sup>55</sup>

Information. Low-resolution current density maps displaying only the planar regime on  $\sigma_h$  are insufficient to visualize the local regime. The analysis of the eigenvalues of the Jacobian matrix, eq 1, and a blow-up of this figure are required to reveal the presence of the foci, see the Supporting Information of a previous paper.<sup>24</sup>

One could hardly find a better proof that *spatial* RCMs, illustrated in Figures 1 and 2, are needed to understand the magnetic response of cyclopropane.<sup>55</sup>

#### 4. Merging of Vortex and Saddle Flow in Cyclopropane

FBL proposed a model merging three diatropic bond vortices to interpret the diatropic ring current and the central paratropic vortex observed in their current density maps for cyclopropane.<sup>19</sup> In those maps important patterns were not

shown, e.g., the strong C-centered circulations and the fine structure of the current density field  $J^B$ , whose most striking feature is probably the saddle—rather than vortex—character of the stagnation points close to the midpoints of the C–C bonds, as already reported in previous papers.<sup>26,24</sup> Thus a different model is required to get a qualitatively correct representation of  $J^B$  of cyclopropane, allowing for the stagnation graph of Figure 1 and the pseudostagnation graph of Figure 3. In the latter, the isolated  $(3, \pm 1)$  SPs are connected by continuous paths of points at which the out-of-plane  $J_z^B \neq 0$ , whereas the modulus of the in-plane current  $J_{xy}^B$  vanishes. For that reason these paths are called pseudostagnation lines.

Starting from examination of  $J^B$  far from the molecular plane in Figure 1, the set of one central SL and six pseudostagnation lines can be interpreted in terms of a basic

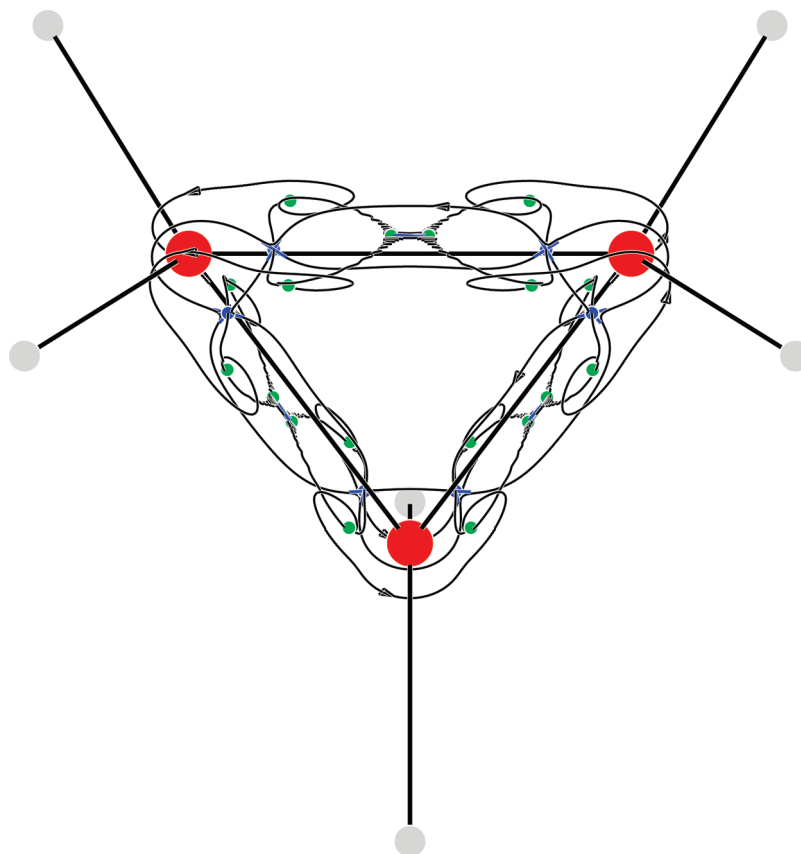


**Figure 2.** Spiral flow connecting the 18 isolated  $(3, \pm 1)$  foci (in green) and the 6 isolated  $(3, \pm 1)$  saddle nodes (in blue, marked by a cross) in the C–C bond regions of cyclopropane in a magnetic field  $B_{\parallel}$ .

center–saddle–center pattern roughly above a C–C bond; that pattern is consistent with the summation of two separated diatropic C-centered vortices.<sup>57</sup> Nonetheless, further investigation requires the analysis of the isolated SPs.

The 6 foci and 6 saddle nodes on the C-plane as well as the 12 out-of-plane foci have a three-dimensional nature; as all of the eigenvalues of their Jacobian are nonzero, they should be analyzed in terms of genuine three-dimensional fields, which excludes the possibility of taking sums of purely rotational fields as in a previous paper.<sup>57</sup> However, an analogous analysis is possible by formally setting  $J_z^{\mathbf{B}} = 0$  and considering only the field over the  $xy$  plane,  $\mathbf{J}_{xy}^{\mathbf{B}} = J_x^{\mathbf{B}}\mathbf{e}_1 + J_y^{\mathbf{B}}\mathbf{e}_2$ , which is sufficient to determine the magnetic properties, although it has nonzero divergence due to the cancellation of the  $J_z^{\mathbf{B}}$  component.

The isolated  $(3, \pm 1)$  SPs and the  $(2,0)$  saddle SLs of the  $\mathbf{J}^{\mathbf{B}}$  field are also present in the  $\mathbf{J}_{xy}^{\mathbf{B}}$  field. However, in the pseudostagnation graph for the latter in Figure 3, the isolated single points are connected by six closed pseudostagnation loops, symmetrically placed on both sides of each true saddle line intersecting  $\sigma_h$  about the midpoint of a C–C bond, see also Figure 1. The pseudostagnation loops lie inside domains bounded by asymptotic streamlines shown in Figure 2. In the following we will assume, without loss of accuracy, that the  $(3, \pm 1)$  saddle nodes (foci) can be treated as planar saddles (centers), which is consistent with the fact that the small local  $J_z^{\mathbf{B}}$  component is neglected. We have accordingly found that each of the three pairs of stagnation loops of  $\mathbf{J}_{xy}^{\mathbf{B}}$  in Figure 3 can be interpreted in terms of three diatropic

circulations: two of them being centered on the C atoms and one on the C–C bond.

To obtain this result, we have considered the summation of three purely rotational two-dimensional diatropic vortices with  $(x, y)$  centers in  $(R_1, 0)$ ,  $(R_2, 0)$  and  $(R_3, 0)$  and the general expression  $\mathbf{J}^{\mathbf{B}(i)} = J^{\mathbf{B}(i)}(r_i)\hat{\theta}_i$ , where the  $J^{\mathbf{B}(i)}(r_i)$  functions vanish only at 0 and  $\infty$ ,  $i = 1, 2$ , and 3, and  $r_i$  and  $\theta_i$  are the polar coordinates with respect to the  $i$ -th center. The three components  $J_x^{\mathbf{B}(i)}$  have the same sign above and below the  $x$  direction, where they vanish. Therefore, stagnation points can only be found on the  $x$  axis if the three components  $J_y^{\mathbf{B}(i)}$  cancel out. Assuming real (imaginary) eigenvalues for the two-dimensional Jacobian leads to the conclusion that a stagnation point will be a saddle (vortex) if

$$\frac{\partial |J_{\theta}^{\mathbf{B}(1)}|}{\partial r_1} - \frac{\partial |J_{\theta}^{\mathbf{B}(2)}|}{\partial r_1} - \frac{\partial |J_{\theta}^{\mathbf{B}(3)}|}{\partial r_1}$$

is negative (positive). This condition reduces to that previously analyzed for two circulations if  $|J_{\theta}^{\mathbf{B}(2)}| = 0$ .<sup>57</sup>

The shape of the  $J_{\theta}^{\mathbf{B}(i)}$  functions is clearly a crucial factor for determining the overall pattern. The ab initio current density can in general be expressed as a sum of Gaussian terms.<sup>57</sup> However, for the sake of simplicity, we will make use here of a single exponential form. The form chosen is  $J_{\theta}^{\mathbf{B}(i)} = I_i N_i r_i^2 \exp(-a_i r_i^2)$ , where the shape of the function is determined by two parameters,  $a_i$  and  $I_i$ , and the normalization constant is  $N_i = 1/\int_0^{\infty} r_i^2 \exp(-a_i r_i^2) dr_i$ . We have first considered the summation of three identical circulations of

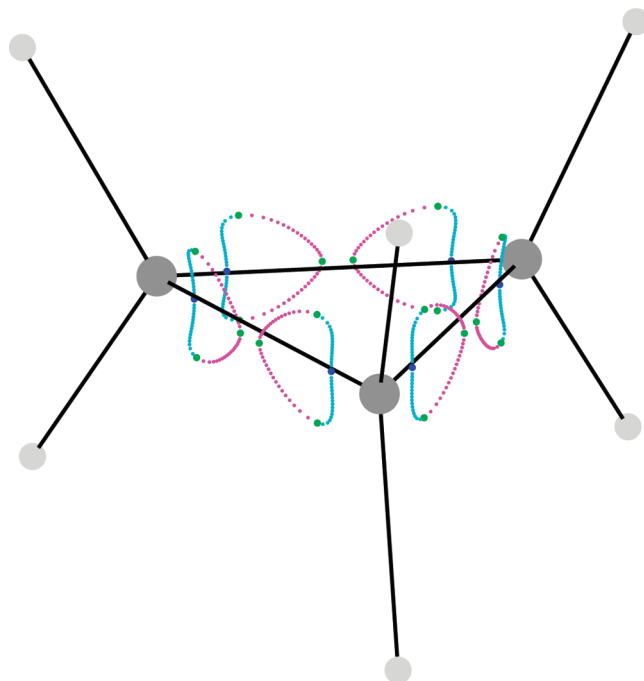


**Figure 3.** Pseudostagnation graph of the planar  $\mathbf{J}_{xy}^B$  field. The closed loops are continuous paths of points at which the modulus  $|\mathbf{J}_{xy}^B| = 0$ . They contain  $(3, \pm 1)$  isolated points, observed also in Figures 1 and 2, where the total current density  $|\mathbf{J}^B|$  vanishes. Green (blue) dots correspond to foci (saddle nodes). Magenta (cyan) paths indicate that spiral (saddle) flow is observed on  $\mathbf{J}_{xy}^B$  cross-sectional streamline plots parallel to  $\sigma_h$ . The seven SLs characterizing the  $\mathbf{J}^B$  field, see Figure 1, have been omitted for clarity.

unitary intensity  $I$  placed at  $-0.75$ ,  $0$ , and  $0.75$  Å on the  $x$  axis. Figure 4 shows that, on changing the common  $a$  parameter, the number and type of the stagnation points changes. Starting from a single center for very broad functions (small  $a$ ) and sharpening the  $J_{\theta}^{B(i)}$  functions, one gets three stagnation points, corresponding to two circulations separated by a saddle. For still sharper functions, seven stagnation points appear: four circulations separated by three saddles, as found on the molecular plane of cyclopropane.

Setting now  $a_1 = a_2 = a_3 = 10$  Å $^{-2}$ , a value at which the 7 stagnation points occur, we have investigated the behavior of the pseudostagnation lines on moving further from the molecular plane. To simulate the fact that C-centered circulations, sustained by the C–H electron density, extend higher than the bond-centered circulations, we varied the intensity of the central flow. Figure 5 displays the position and the nature of the stagnation points as the intensity  $I_2$  is changed from  $0$  to  $2I_1$ . The vertical axis has been reversed to make easier the comparison with Figure 3. It can be seen that, for a low intensity of the central circulation, the current pattern is substantially that expected for only two separated homotropic circulations.

However when the strength of the central flow is comparable with that of the circulations nearby, the pattern of seven stagnation point starts to appear. Upon further increase, the central circulation dominates the current pattern, although the presence of the circulations at its sides can still be predicted from the three center–saddle–center stagnation

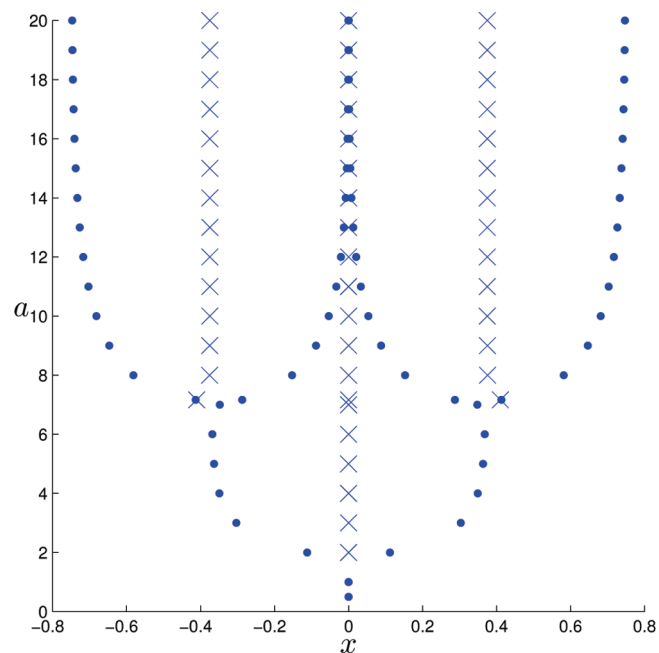


**Figure 4.** Nature and location of the stagnation points of the  $\mathbf{J}_{xy}^B$  field obtained by summing three collinear diatropic vortices of equal shape and intensity, placed at  $x = -0.75$ ,  $0$ , and  $0.75$  Å. The computations were repeated for different values of the exponent  $a$  (see text). Centers and saddles are indicated by • and ×, respectively.

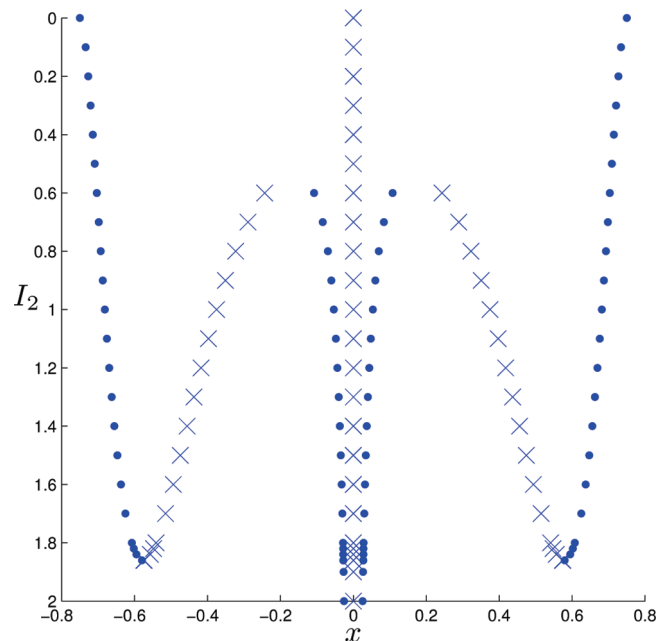


**Figure 5.** Nature and location of the stagnation points of the  $\mathbf{J}_{xy}^B$  field obtained by summing three collinear diatropic vortices located, as in Figure 4, and with  $a = 10$  Å $^{-2}$ . The computations were repeated for different values of the  $I_2/I_1$  ratio. Centers and saddles are indicated by • and ×, respectively.

points close to  $x = 0$ , rather than a single center. The upper part of Figure 5, with the disappearance of four stagnation points, nicely parallels the pseudostagnation graph of the  $\mathbf{J}_{xy}^B$  field displayed in Figure 3.

## 5. Magnetic Response Tensors of Cyclopropane

Attempts are usually made to infer molecular current density models by experimental values of magnetic susceptibility<sup>12</sup> and NMR chemical shift<sup>58</sup> as well as nonmeasurable NICS.<sup>13,14</sup> However, it is not possible, in general, to construct a plausible global model of  $\mathbf{J}^B$  field only allowing for a few numbers. Just the other way around, one can reasonably argue that a *falsifiable* current density model should be developed in advance. After any possible tests on its ability to rationalize all available data, such a model is accepted or rejected. Improved versions can later be sought, still requiring their falsifiability.

Therefore, we find it expedient to start by defining the magnetic properties of a molecule in terms of the quantum mechanical induced current density. When the *subobservable*<sup>59</sup>  $\mathbf{J}^B$  is available, one can treat it as a completely classical quantity, forgetting about the quantum mechanical procedure used to obtain it and rely on the law of classical electrodynamics for the interpretation of magnetic response.

Denoting by  $\epsilon_{\alpha\beta\gamma}$  the Levi–Civita unit tensor and using the implicit summation rule for repeated suffixes according to tensor notation, the orbital magnetic dipole moment induced in the  $n$  electrons of a molecule by an external magnetic field with flux density  $\mathbf{B}$  is evaluated by the Ampere law assuming linear response:

$$\Delta\langle m_\alpha \rangle = \chi_{\alpha\beta} B_\beta = -\frac{1}{2}\epsilon_{\alpha\beta\gamma} \int J_\beta^B(\mathbf{r}) r_\gamma d^3r \quad (2)$$

The magnetic field induced at an observation point  $\mathbf{R}$  is determined by the Biot–Savart law:

$$\Delta\langle B_\alpha^n(\mathbf{R}) \rangle = -\sigma_{\alpha\beta}(\mathbf{R}) B_\beta = \frac{\mu_0}{4\pi} \epsilon_{\alpha\beta\gamma} \int J_\beta^B(\mathbf{r}) \frac{R_\gamma - r_\gamma}{|\mathbf{R} - \mathbf{r}|^3} d^3r \quad (3)$$

Introducing the current density tensor<sup>60</sup> via the derivative:

$$\mathcal{J}_\alpha^B(\mathbf{r}) = \frac{\partial}{\partial B_\beta} J_\alpha^B(\mathbf{r}) \quad (4)$$

the magnetizability tensor is evaluated by

$$\chi_{\alpha\delta} = \frac{1}{2} \epsilon_{\alpha\beta\gamma} \int r_\beta \mathcal{J}_\gamma^B(\mathbf{r}) d^3r \quad (5)$$

and the shielding tensor at  $\mathbf{R}$  is obtained as

$$\sigma_{\alpha\delta}(\mathbf{R}) = -\frac{\mu_0}{4\pi} \epsilon_{\alpha\beta\gamma} \int \frac{r_\beta - R_\beta}{|\mathbf{r} - \mathbf{R}|^3} \mathcal{J}_\gamma^B(\mathbf{r}) d^3r \quad (6)$$

If  $\mathbf{R}$  coincides with the position  $\mathbf{R}_I$  of the  $I$ -th nucleus, carrying an intrinsic magnetic dipole  $m_{I\alpha}$ , the quantity  $\sigma_{\alpha\beta}(\mathbf{R}_I) \equiv \sigma_{\alpha\beta}^I$  defines the magnetic shielding tensor of that nucleus. The integrand function is interpreted as a shielding density second-rank tensor,<sup>61,62</sup> for instance

$$\Sigma_{zz}^I(\mathbf{r}) = -\frac{\mu_0}{4\pi} \epsilon_{z\beta\gamma} \frac{r_\beta - R_{I\beta}}{|\mathbf{r} - \mathbf{R}_I|^3} \mathcal{J}_\gamma^B(\mathbf{r}) \quad (7)$$

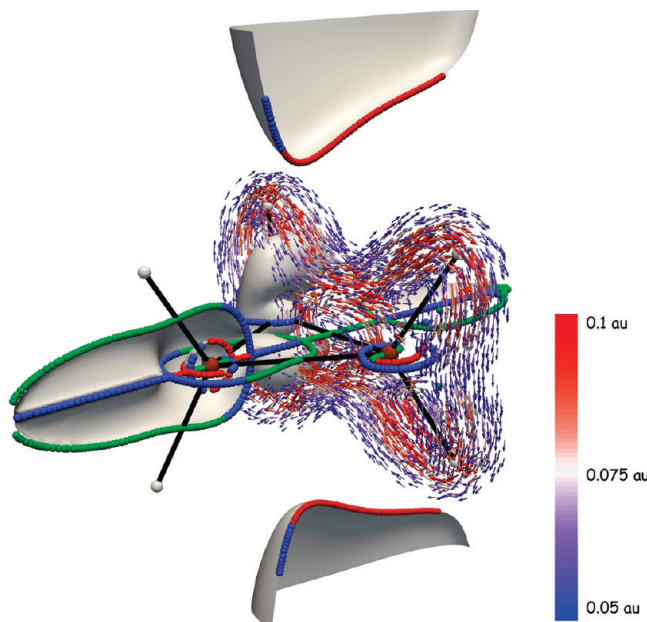


**Figure 6.** The strong “ring current” flowing around the  $\text{CH}_2-\text{CH}_2$  fragment of the cyclopropane molecule in a magnetic field of 1 au, applied along the  $C_2 \equiv x$  symmetry axis. Only current densities with  $|J^B|$  between 0.05 (blue arrows) and 0.1 au (red arrows) are plotted. The maximum modulus is  $\approx 0.11$  au. The gray surfaces represent isoshielding density regions  $\Sigma_{xx}^I(\mathbf{r}) = 0.0$  au, for any ghost atom  $I$  along the  $C_2$  axis. Vortical and saddle stagnation lines lie on these surfaces, see also Figure 7.

is the  $zz$  component of the shielding density for nucleus  $I$  at a point  $\mathbf{r}$  in a given domain.

This function is usually plotted over a plane, as in Figures 11 and 12, to analyze shielding/deshielding mechanisms operating in different basins of the current density field via a few prescriptions illustrating the effect of  $\mathbf{J}^B$  at point  $\mathbf{r}$  on  $\Sigma_{zz}^I(\mathbf{r})$ .<sup>49</sup> Isoshielding density surfaces can also be visualized, see Figures 7 and 8. Although *all* the planes perpendicular to a given direction, e.g.,  $z$ , provide an infinitesimal “slice” contribution to the total induced field (eq 6), in practice one does not need to examine the density (eq 7) over a large number of plot planes. Usually only a few are taken into account, those from which sizable contributions are expected to arise, e.g., planes of nearly maximum charge distribution can be sampled.

It is important to recall that the induced orbital moment (eq 2) and the magnetic susceptibility (eq 5) are *global* properties, proportional to the area enclosed by a wide domain of induced current loops,<sup>63</sup> whereas the magnetic shielding (eq 6) at  $\mathbf{R}$  is mainly determined by the flow in a small region about the probe, as it depends on the second inverse power of the distance  $|\mathbf{r} - \mathbf{R}|$  from the observation point. Therefore the components of the magnetic tensors  $\chi_{\alpha\beta}$ ,  $\sigma_{\alpha\beta}^I$ , and possibly NICS, provide different, complementary pieces of information.

Near Hartree–Fock CTOCD estimates of the magnetic susceptibility  $\chi_{\alpha\beta}$  and nuclear shieldings  $\sigma_{\alpha\beta}^I$  of cyclopropane have recently been reported using an extended (13s10p5d2f/8s4p1d) basis set containing 435 primitive Gaussian functions. Calculations were carried out by the SYSMO computer

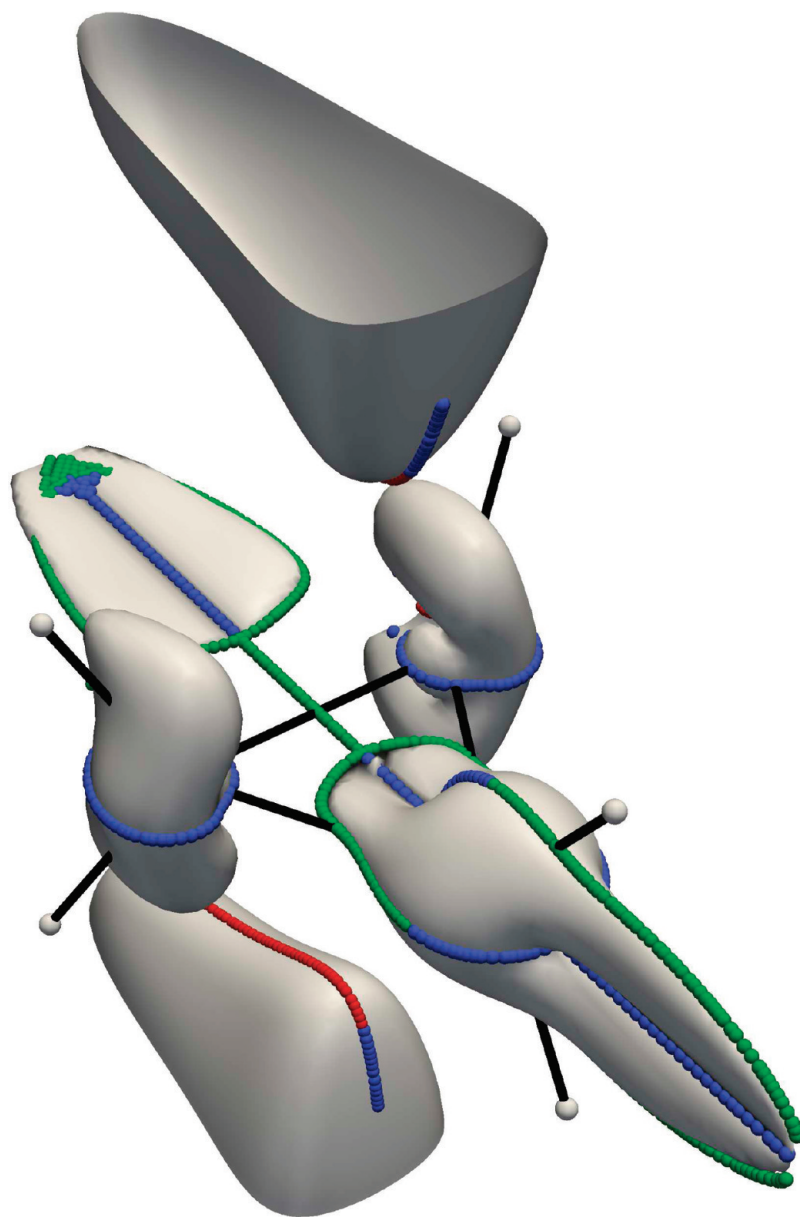


**Figure 7.** The stagnation graph of cyclopropane in a magnetic field parallel to the  $C_2 \equiv x$  symmetry axis. The stagnation lines lie on isoshielding density surfaces  $\Sigma'_{xx}(\mathbf{r}) = 0.0$  au, represented in gray, for any dummy atom  $I$  along  $C_2$ .

code.<sup>64</sup> The high quality of the calculations was assessed by a number of criteria.<sup>24</sup> It should be emphasized that the magnetic tensors of cyclopropane calculated by CTOCD procedures are invariant in a gauge translation.<sup>60,65,37</sup> The RCM developed in the present paper is required to explain sign and magnitude of the diagonal components of these tensors and to elucidate the source of their strong anisotropy by applying a few simple rules outlined hereafter.

According to eqs 2–6, the electronic magnetic moment  $\Delta\langle m_a \rangle$  and the magnetic field  $\Delta\langle B_z^n(\mathbf{R}) \rangle$  induced at position  $\mathbf{R}$  by an external field  $B_z$ , the magnetizability component  $\chi_{zz}$ , and the nuclear shielding component  $\sigma_{zz}(\mathbf{R})$  are determined only by the components  $J_x^{\mathbf{B}}$  and  $J_y^{\mathbf{B}}$  of the current density in the  $xy$  plane. The paramagnetic component  $J_z^{\mathbf{B}}$  has no effect on  $\chi_{zz}$  and  $\sigma_{zz}(\mathbf{R})$ . These statements are valid for cyclic permutations of  $x$ ,  $y$ , and  $z$ .

The diatropic electronic ring currents flowing in planes parallel to the  $\sigma_h \equiv \sigma_{xy}$  plane of a conjugated cyclic molecule

in the presence of a magnetic field  $B_z$ : (i) exalt the out-of-plane component  $\chi_{zz}$  of the magnetic susceptibility, and consequently increase the magnitude of the anisotropy  $\Delta\chi$  and the average magnetic susceptibility  $\chi_{av}$  and (ii) enhance (diminish) the out-of-plane component  $\sigma_{zz}^I$  of a real or dummy nucleus  $I$ , placed at  $\mathbf{R}_I$ , inside (outside) the ring. In correspondence with the increase (decrease) of  $\sigma_{zz}^I$ , one observes an upfield (downfield)—also called diamagnetic (paramagnetic)—contribution to the NMR chemical shift from a reference compound, usually tetramethylsilane (TMS),  $\delta^I = \sigma_{av}^{\text{ref}} - \sigma_{av}^I$ . By reversing the direction of  $\mathbf{J}^{\mathbf{B}}$ , i.e., for a paratropic current, the sign of the contributions mentioned above is also reversed.

A familiar example widely discussed in the literature is benzene, whose  $\pi$ -ring currents determine observable effects: high anisotropy  $\Delta\chi$ , big  $\chi_{av}$ , and downfield chemical shift of protons as well as a big positive value of the average

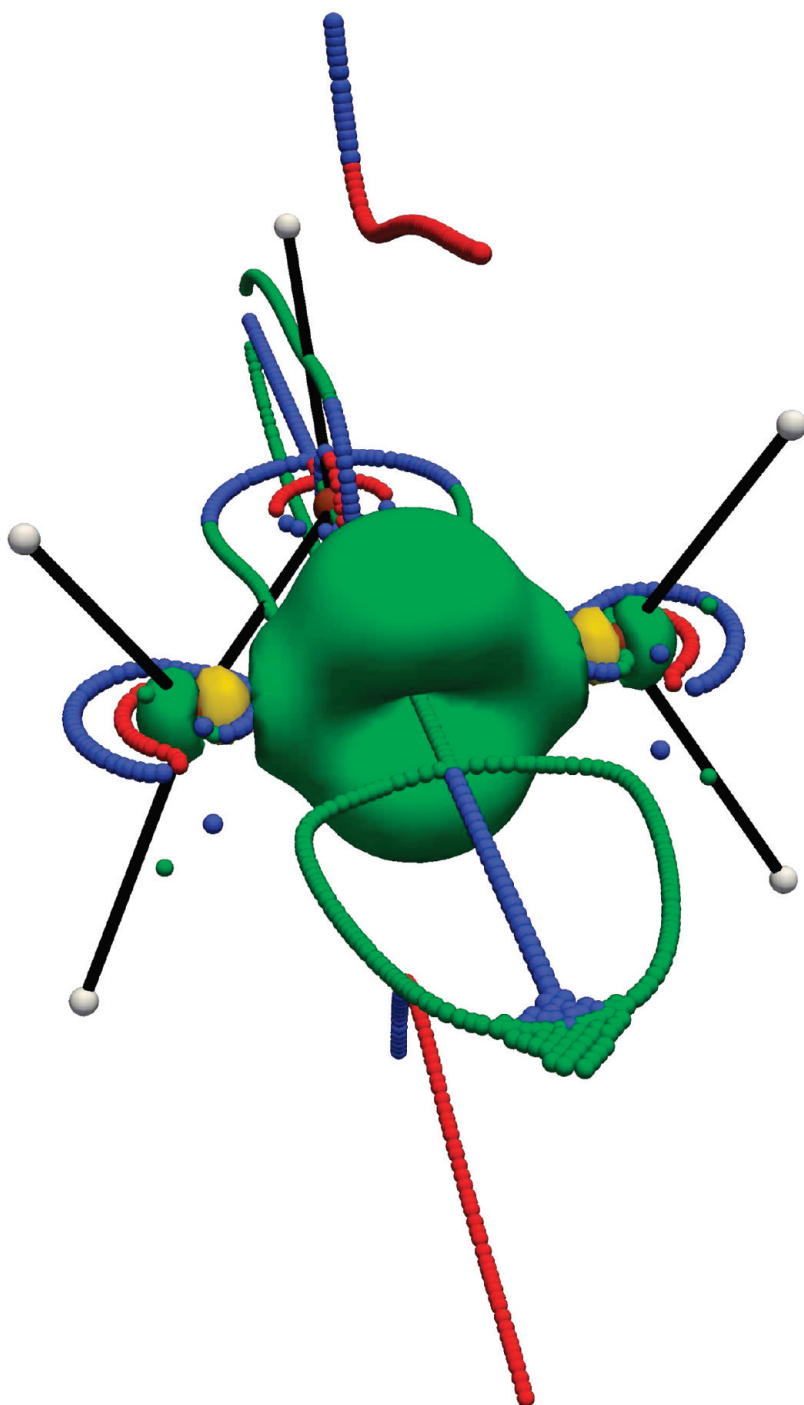


**Figure 8.** Isoshielding density surface  $|\Sigma'_{xx}(\mathbf{r})| = 0.05 \text{ au}$ , for a dummy atom  $I$  at the midpoint of a C–C bond. Green (yellow) portions denote positive diamagnetic (negative paramagnetic) contributions.

central shielding, or a big negative average NICS, which is defined as the same quantity with negative sign.<sup>13</sup>

However, it should be emphasized that the ring currents can only bias the out-of-plane component of the magnetic tensors of conjugated planar (poly)cyclic molecules. Properties observed in systems in disordered phase account for only one-third of the effect arising from the ring currents. Sizable, or sometimes overwhelming contributions from mechanisms other than ring currents, affecting the in-plane components of the magnetic tensors, should carefully be examined, and any theoretical assessment of

the strength of delocalized ring currents in planar conjugated carbon cycles should take only the out-of-plane components  $\chi_{zz}$  and  $\sigma_{zz}^I$  into account.<sup>66</sup>

For a ghost atom  $I$ , with coordinate  $\mathbf{R}_I$ , placed anywhere along the  $C_3 \equiv z$  symmetry axis of  $\text{C}_3\text{H}_6$ , the equation  $\Sigma'_{zz}(\mathbf{r}) = 0$  defines a surface of points  $\mathbf{r}$  of vanishing shielding density. The same statement holds for  $\Sigma'_{xx}(\mathbf{r}) = 0$ , with  $I$  a dummy atom along the  $C_2 \equiv x$  symmetry axis. Stagnation lines lie on the zero-isoshielding surfaces, as shown in Figure 6 by superimposing the stagnation graph to some portions of the  $\Sigma'_{xx}(\mathbf{r}) = 0$  domain. Another view of this pattern is

observed in Figure 7 for all dummy atoms  $I$  lying on  $C_2$ , with arbitrary  $\mathbf{R}_I$ .

Abnormally high calculated values of average NICS<sup>13</sup> are considered to be consistent with  $\sigma$ -diatropicity of  $C_3H_6$ .<sup>28,29,34,35</sup> In fact, cyclopropane provides crucial evidence on the failure of the average NICS<sup>13</sup> as a measure of diatropicity.<sup>24</sup> The calculated NICS  $\equiv -\sigma_{av}^{CM}$  is as big as  $-44.9$  ppm, a value comparable with the GIAO NICS RHF/6-311+G(d,p) estimate  $-43.0$  given by Sauers,<sup>35</sup> and with similar values by others.<sup>28,34</sup> Noticeably enough,  $\sigma_{av}^{CM}$  is dominated by the enormous in-plane component  $\sigma_{||}^{CM} = 50.9$  ppm, a case predicted in a previous paper.<sup>66</sup> The out-of-plane  $\sigma_{\perp}^{CM}$  component is  $\approx 18$  ppm smaller. Therefore, neither the average NICS<sup>13</sup> nor NICS<sub>||</sub><sup>66,67</sup> can be used as magnetic aromaticity quantifiers in cyclopropane.

This peculiarity of  $C_3H_6$  is explained by the RCM developed here. In a field  $B_{\perp}$  applied in the direction of a  $C_2$  symmetry axis, intense delocalized currents (with maximum modulus  $\approx 0.11$  au for an applied magnetic field of 1 au) take place in the bent “banana bond” lying outside of the direction interconnecting two carbon nuclei,<sup>68</sup> and about the C–H bonds, as shown by Figure 6 in the text and Figure 6 in the Supporting Information. It is this current, with strength 15.7 nA/T (evaluated as a flux integral over a suitably defined “bond basin” in Section 6), flowing around the  $CH_2-CH_2$  and methylene moieties that determines the huge value of the  $\sigma_{\perp}^{CM}$ .

Quite remarkably, a similar pattern was observed for ethylene, another noncyclic system which sustains an annular weaker current (with modulus 0.075 au, for  $|B| = 1$  au) on the molecular plane, see Figure 12 of a previous article.<sup>69</sup> The SG of the ethylene molecule in a magnetic field perpendicular to  $\sigma_h$ , see Figure 6 of the same paper<sup>69</sup> contains loops similar to those observed in the vicinity of the C nuclei in Figure 6.

It may be useful to complete the analysis of the different contributions to the central shielding (and NICS) values calculated for cyclopropane by comparison with corresponding data for benzene. Allowing for a calculation adopting the same basis set for the sake of consistency,<sup>48</sup> we obtained  $\sigma_{\perp}^{CM} = 5.38$ ,  $\sigma_{||}^{CM} = 18.40$ , and  $\sigma_{av}^{CM} = 9.72$  ppm for  $C_6H_6$ . The  $\sigma$  and  $\pi$  contributions to the out-of-plane component, determined by conflicting mechanisms, are  $-18.86$  and  $37.26$ , respectively (all values in ppm). Therefore, even if the  $\sigma_{||}^{CM} = 32.69$  ppm is smaller than  $\sigma_{\perp}^{CM}$  for cyclopropane, it is far larger than that for benzene and only 4.57 ppm smaller than the dominant  $\pi$ -contribution to benzene’s  $\sigma_{||}^{CM}$ .

Recalling that the shielding density of a probe depends on the second inverse power of its distance from an element of current, according to the Biot–Savart law (eq 3), we conclude that total calculated  $\sigma_{||}^{CM}$  values for the two molecules should be rationalized in terms of: (i) comparable values of  $|J^B|$ , but (ii) different spatial extensions of the integration domains, and (iii) competing  $\sigma$ - and  $\pi$ -electron flow in benzene, which are absent in cyclopropane.

These results indicate that any conclusion on relative magnetic aromaticity in benzene and cyclopropane based on  $\sigma_{||}^{CM}$  (and NICS<sub>||</sub>) values would not make sense.

## 6. Integrated Current Densities

The divergence of the stationary current density vector vanishes everywhere. Then, according to the Gauss theorem, also the flux  $\Phi$  of the  $\mathbf{J}^B$  field vanishes for any closed surface  $S$  enclosing the volume  $V$ :

$$\Phi = \int_S \mathbf{J}^B \cdot d\mathbf{s} = \int_V \nabla \cdot \mathbf{J}^B dv = 0 \quad (8)$$

From this relationship, it is easy to show (see a forthcoming paper on the  $\pi$  character of ring current in aromatics)<sup>33</sup> that the integral of the current density crossing *any* arbitrarily chosen plane  $P$  bisecting the molecular domain vanishes:

$$\int_P \mathbf{J}^B \cdot d\mathbf{p} = 0 \quad (9)$$

In actual calculations,  $\nabla \cdot \mathbf{J}^B$  is not zero, and eq 9 is not exactly fulfilled, except for symmetry reasons, e.g., for all planes containing an  $n$ -even symmetry axis  $C_n$  parallel to the inducing magnetic field  $\mathbf{B}$ , and for a symmetry plane perpendicular to  $\mathbf{B}$ . In general, the magnitude of the integral in eq 9 approaches zero on improving the quality of the calculation.

However, the integral in eq 9 is different from zero when  $P$  is a bounded portion of a plane, thus a measure of the strength of delocalized currents is assumed to be given by the flux of the  $\mathbf{J}^B$  vector through a suitably selected planar domain. For symmetric cyclic hydrocarbons, the halfplane bounded by the symmetry axis and bisecting a CC bond is a convenient choice of  $P$  to evaluate current strengths, also referred to as bond current susceptibilities.<sup>27,70–72</sup>

In the case of benzene and other  $\pi$ -diatropic systems in a magnetic field  $\mathbf{B}$  at right angles to the molecular plane, *all* the streamlines of the  $\pi$ -current enter in the same direction the domain  $P$  of the integral  $\int_P \mathbf{J}^B \cdot d\mathbf{p}$  defining the current strength. The largest  $|J^B|$  modulus values of the  $\pi$ -current of benzene are observed inside two toroidal regions of higher  $\pi$ -electron density, above and below the  $\sigma_h$  plane.<sup>70</sup> The  $\pi$ -currents flowing inside these Farnum–Wilcox tori<sup>73</sup> give an overwhelming contribution to the total current strength  $\int_P \mathbf{J}^B \cdot d\mathbf{p}$ .

On the other hand, the  $\sigma$  currents of most conjugated cyclic molecules, including benzene, are diatropic (paratropic) outside (inside) the ring.<sup>48</sup> Moreover, disconnected domains with the same regime frequently occur, which makes the definition of  $P$  more complicated. This is the case of cyclopropane, as observed for  $B_{||}$  in Figure 9, which shows the cross-section of the induced current density modulus on a plane bisecting a C–C bond. The calculated current strength is 10.2 nA/T, the diatropic (paratropic) contribution being 11.6 ( $-1.4$ ) nA/T. These estimates virtually coincide with those of a previous paper.<sup>27</sup>

Figure 9 documents the effect of an intense diatropic circulation, with the shape of a topological torus, embedding the entire molecule. Such a ring current is sustained by delocalized  $\sigma$ -electrons shared by the three carbon atoms, as claimed by Dale Poulter et al.,<sup>7</sup> and also by the hydrogen atoms. Therefore, one should not limit himself to consider the effect of electrons precessing in a *circle* which circumscribes the ring.<sup>7</sup> The magnetic response of cyclopropane to

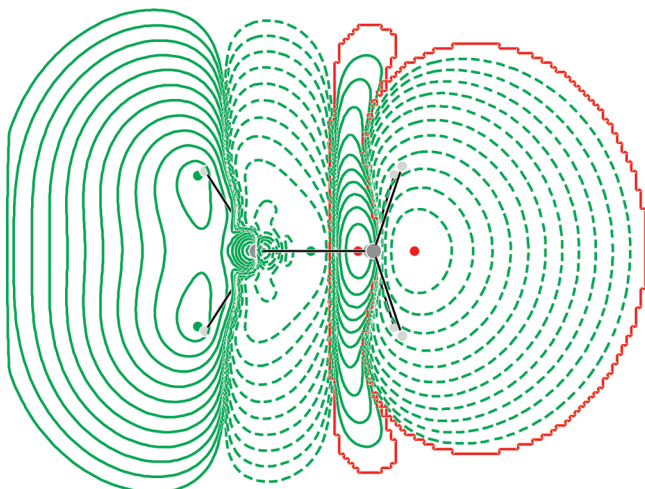


**Figure 9.** Contour plot of the cross-section of the current density modulus  $|J^B|$  on a  $14 \times 14$  bohr region of the  $xz$  plane spanned by the  $C_2 \equiv x$  and the  $C_3 \equiv z$  symmetry axes, bisecting a C–C bond. The applied magnetic field  $B_z$ , of magnitude 1 au, is orthogonal to the  $\sigma_h \equiv xy$  symmetry plane. The H and C nuclei are represented in two shades of gray. Solid and dashed lines denote flow in opposite directions. Within the integration domain  $P$ , bounded by the red frontier, paratropic (diatropic) currents correspond to solid (dashed) contours. Red and green dots indicate extreme values of  $|J^B|$  on the plot plane,  $|J^B|_{\max} = 0.054$  ( $|J^B|_{\max}^d = 0.128$ ) au for the internal paratropic (external diatropic) flow. Contour values decrease in steps of  $|J^B|_{\max}/2n$ , for  $n = 1, 2, \dots$ . The total current strength, defined as the flux integral  $\int_P J^B \cdot d\mathbf{p}$  from the domain within the red boundary, is 10.235 nA/T. The contributions from external (diatropic) and internal (paratropic) flow are 11.619 and  $-1.384$  nA/T, respectively. Here, and in Figure 10, calculated current strengths do not show significant changes on enlarging the integration domain.

a magnetic field orthogonal to the carbon plane should more properly be interpreted in terms of a delocalized *toroidal* current flowing around carbon and hydrogen atoms.

The calculated current strength for  $B_\perp = 1$  au, see Figure 10, is 15.7 nA/T, i.e.,  $\approx 1.5$  times higher than that calculated for  $B_{||}$ . The huge value of the  $\sigma_\perp^{\text{CM}} = 50.9$  ppm is biased to a great extent by this peculiar “delocalized current without a carbon ring”, see also Figure 6 in the Supporting Information.

## 7. Rationalization of Magnetic Shieldings in Cyclopropane via Spatial RCMs

According to Fliegl et al., it is the ring strain that makes the cyclopropane electrons mobile, resulting in a strong magnetic ring current, which could be called “ring-strain current”, affecting magnetic shieldings in the same way as ring currents do.<sup>27</sup> In fact, a ring current flowing in an annular region of the plane of the C nuclei, around the methylene groups, and splitting into two branches along the C–H bonds of cyclopropane in a magnetic field  $B_z$  normal to the molecular plane can be displayed, see Figure 3 of a previous paper,<sup>24</sup> by selecting trajectories with a modulus varying between 0.05 and 0.1 au, for  $B_z$  with strength 1 au, and by cutting currents with much higher intensities in the proximity of the C atoms.

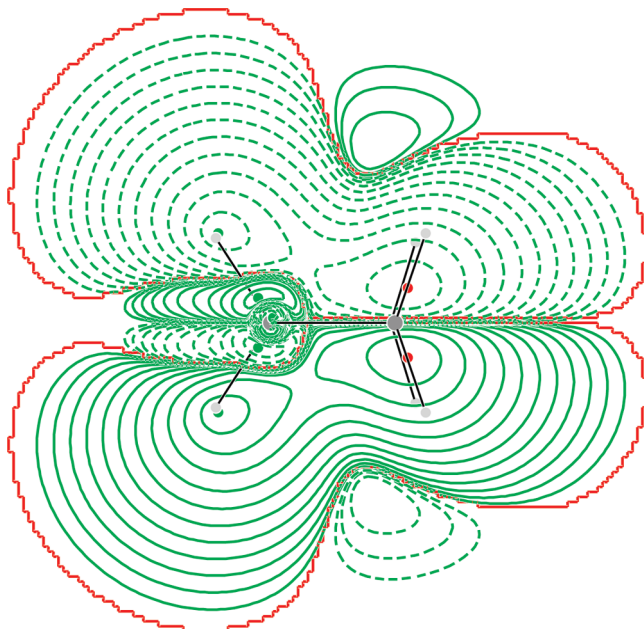


**Figure 10.** Contour plot of the cross-section of the modulus  $|J^B|$  of the current density on the  $xz$  plane spanned by the  $C_2 \equiv x$  and the  $C_3 \equiv z$  symmetry axes, bisecting a C–C bond. The applied magnetic field  $B_x$  lies on the plot plane. The net integrated current strength on the lower (upper) domain with red boundary is +15.663 (-15.663) nA/T.

It is this current that could be referred to as a ring current in the conventional meaning.<sup>7,15</sup> However, it should be emphasized that the shape of the total current density field is that of Figure 1 of the present study, and, accordingly, that both carbon and hydrogen nuclei lie inside a *torus of delocalized currents*. Plots of the shielding density  $\Sigma_{zz}^H$ , eq 7 on four planes, that of the C nuclei at  $z = 0$ , the H nuclei at  $z = 1.702$  bohr, and two intermediate planes at 0.6 and 1.2 bohr are shown in Figure 11. To identify the contributions to proton shielding provided by the delocalized currents and by the local vortices flowing about the  $sp^3$  orbitals forming the C–H bonds, for each plane in that figure, contour levels of  $\Sigma_{zz}^H$  are superimposed to the current density streamlines.

On the  $\sigma_h$  plane pairs of steep up and down spikes of the shielding density function, marked by green and red contours, respectively, are observed about carbon atoms. Their contributions to  $\sigma_{zz}^H$  are virtually vanishing due to cancellation of effects within each pair. On the same plane, a relatively large shielding region extends over the delocalized current domain, whose contribution can be considered minor, or negligible, due to its small magnitude. On going from the plane of the C to that of the H nuclei, both local and nonlocal current domains provide increasingly higher shielding effects of comparable size. A restricted area of deshielding is confined within the domain of local flow. On account of these results, the  $\sigma_{zz}^H$  component is determined by both local and nonlocal currents providing contributions of almost the same order of magnitude. The contribution of the delocalized flow seems slightly dominant owing to its wider extension.

The current density streamlines on the  $\sigma_h$  plane, and three parallel planes at distance 0.2, 0.5, and 0.8 bohr, are superimposed to the out-of-plane component of the shielding density functions,  $\Sigma_{zz}^C$  for carbon in Figure 12 and  $\Sigma_{zz}^I$  for a

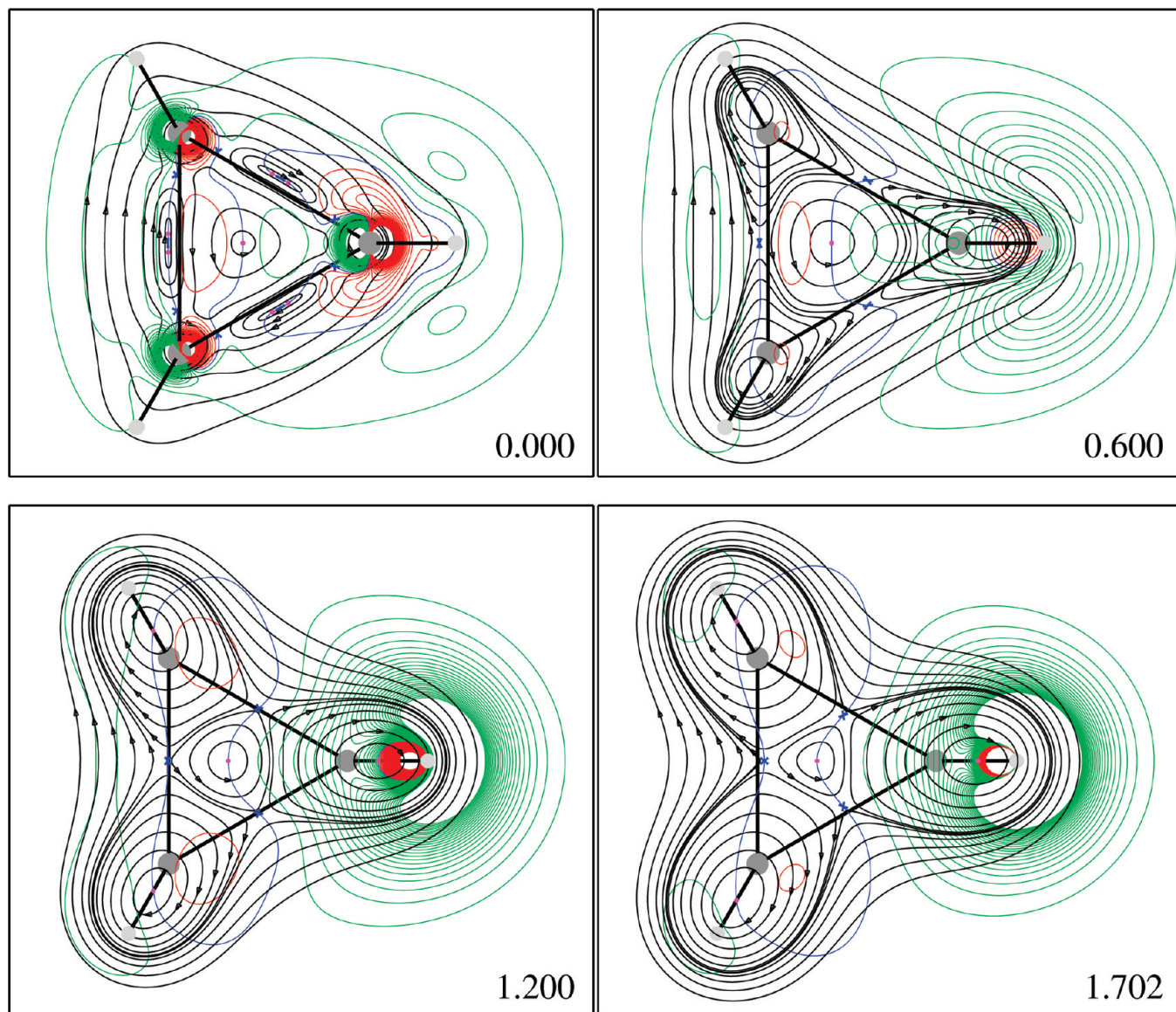


**Figure 11.** Streamlines of  $\mathbf{J}^B$  and corresponding contours of the magnetic shielding density  $\Sigma_{zz}^H$ , in au, for an applied field of 1 au, on the  $\sigma_h$  plane and on three parallel planes at distance (in bohr) 0.6, 1.2, and 1.702 (the plane of the H nuclei). Green (red) contours denote shielding (deshielding). A blue nodal line connects points at which the angle between the local streamline and the direction to the probe is 0 or  $\pi$ , passing through the (2,0) vortex and saddle points on the plot plane, where  $|\mathbf{J}^B|$  vanishes. The nodal line contains also the  $(3, \pm 1)$  saddle nodes and foci on the  $\sigma_h$  plane. The shielding contributions, which arise from the  $\sigma$ -ring currents on the  $\sigma_h$  plane, are very small, those provided by the vortex flowing around the C–H bond and by the delocalized currents increase on the planes at 0.6 and 1.2 bohr and on the plane of the hydrogen nuclei. On these planes, the extension of the domains of delocalized flow providing shielding contributions is higher than that of the local vortex, implying that the former plays a slightly major role. Truncated min, max, and step = −0.05, 0.05, and 0.002 au.

ghost nucleus  $I$  on the center of mass in Figure 13. Let us first consider the  $\Sigma_{zz}^C$  shielding density plot of Figure 12. On the  $\sigma_h$  plane, a major contribution is provided by the diatropic vortex about the carbon atom, where a huge shielding spike is observed, reaching its maximum value within the domain of local current density flow. A sizable contribution arises also from the nearby domain of delocalized current. Pairs of nearly canceling up and down spikes are found on the other carbon atoms. A similar pattern is observed on the plane at 0.2 au. The contributions from the vortex flowing about the C–H bond and from the delocalized currents outside of it decrease on increasing the distance from  $\sigma_h$ . As shown in Figure 12, on the planes at 0.5 and 0.8 bohr, local and

nonlocal domains of flow seem to yield contributions of similar magnitude to  $\sigma_{zz}^C$ . Therefore, one can assert that the out-of-plane component of the carbon shielding is determined by a dominant local contribution and a smaller, non-negligible delocalized contribution.

Then let us consider the  $zz$  component of the central shielding density of Figure 13. On the  $\sigma_h$  plane, pairs of up and down spikes, corresponding to furthest and closest parts of the local C–H bond vortices, are observed about the carbon atoms. They yield negligibly small shielding contributions due to quasi-cancellation for each pair. The strong-deshielding zone confined inside the carbon ring is surrounded by a comparatively weaker-shielding region, spreading

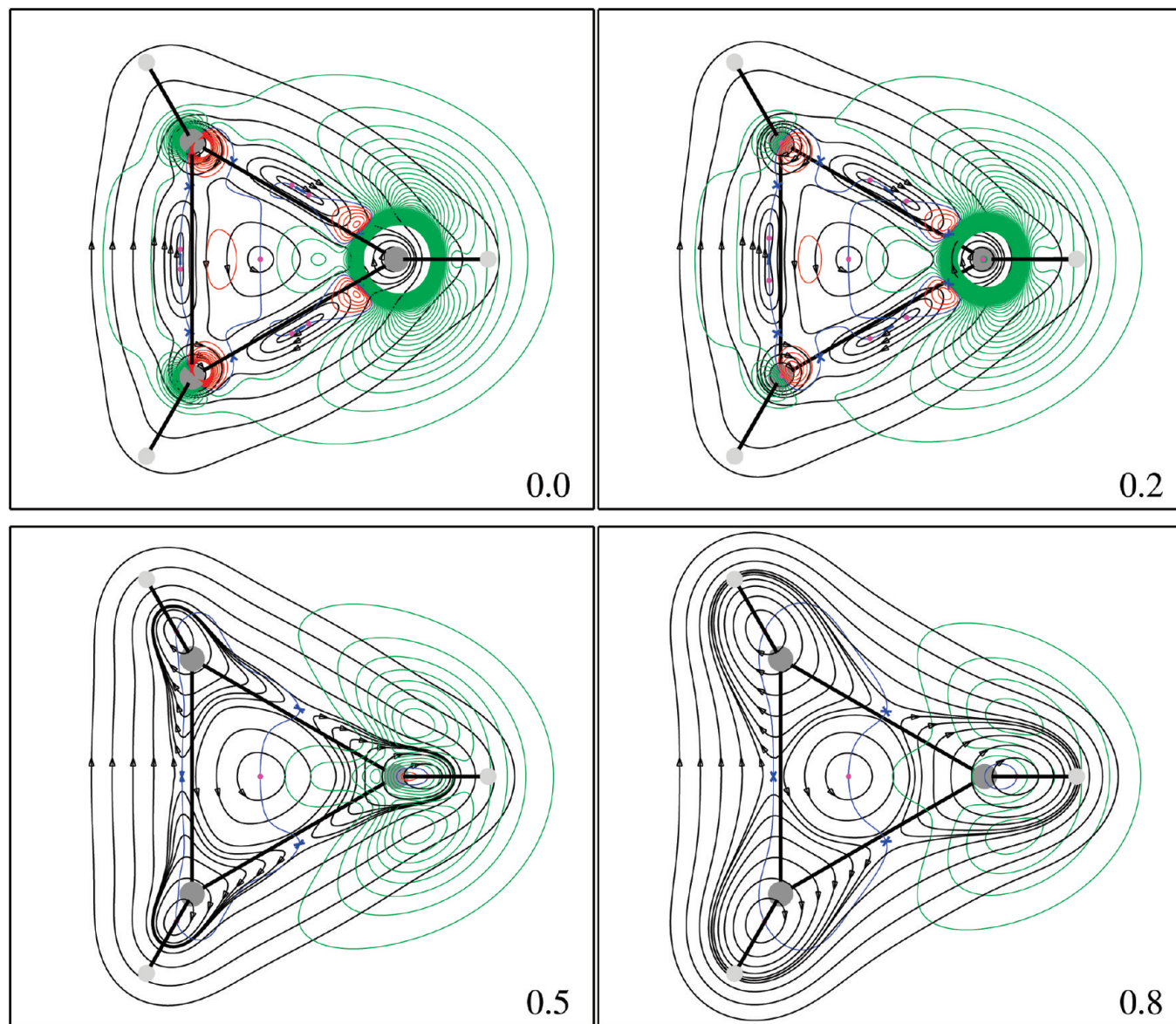


**Figure 12.** Streamlines and corresponding contours of the magnetic shielding density  $\Sigma_{zz}^C$ , in au, for an applied field of 1 au, on the plane of carbon nuclei and on three planes at distance (in bohr) 0.2, 0.5, and 0.8. The color code is the same as in Figure 11. The contributions arising from the vortex flowing around the C–H bond and from the delocalized currents outside of it decrease on increasing the distance from  $\sigma_h$ . Truncated min, max, and step = −0.10, 1.00, and 0.010 au.

however over a much larger area, up to the outer reaches of the  $\sigma_h$  plane, and reaching local maximum values just outside of the C–C bond directions, within the delocalized current domain.

A qualitatively similar pattern is observed on the plane at 0.2 bohr in Figure 13. The magnitude of  $\Sigma_{zz}^{CM}$  decays quite rapidly on more distant planes, relative maxima being still observed for the 0.5 and 0.8 planes in Figure 13, in the region of delocalized regime, in front of the C–C bonds. Therefore, it can be concluded that the large positive value of the out-of-plane component,  $\sigma_{zz}^{CM} = 32.7$  ppm,<sup>24</sup> is determined to a large extent by the dominant shielding contribution provided by the delocalized current flow. Smaller but sizable deshielding contributions are given by the internal paratropic circulation.

## 8. Concluding Remarks

Spatial models of the current density field sustained by the electrons of the cyclopropane molecule in the presence of magnetic fields applied in the directions of either the  $C_3$  or the  $C_2$  symmetry axes, completing and partially revising that recently reported,<sup>24</sup> have been constructed. These models show that a magnetic field  $B_{||}$  along  $C_3$  induces localized vortices enclosed in a toroidal region of delocalized flow, which can be referred to as a spatial “ring current”, circulating beyond the skeleton of C and H nuclei and extending above and below the  $\sigma_h$  plane for more than 1.702 bohr, i.e., the plane of the hydrogen nuclei. Also a magnetic field  $B_{\perp}$  along  $C_2$  induces intense delocalized flow outside of a set of localized vortices, with maximum intensity of

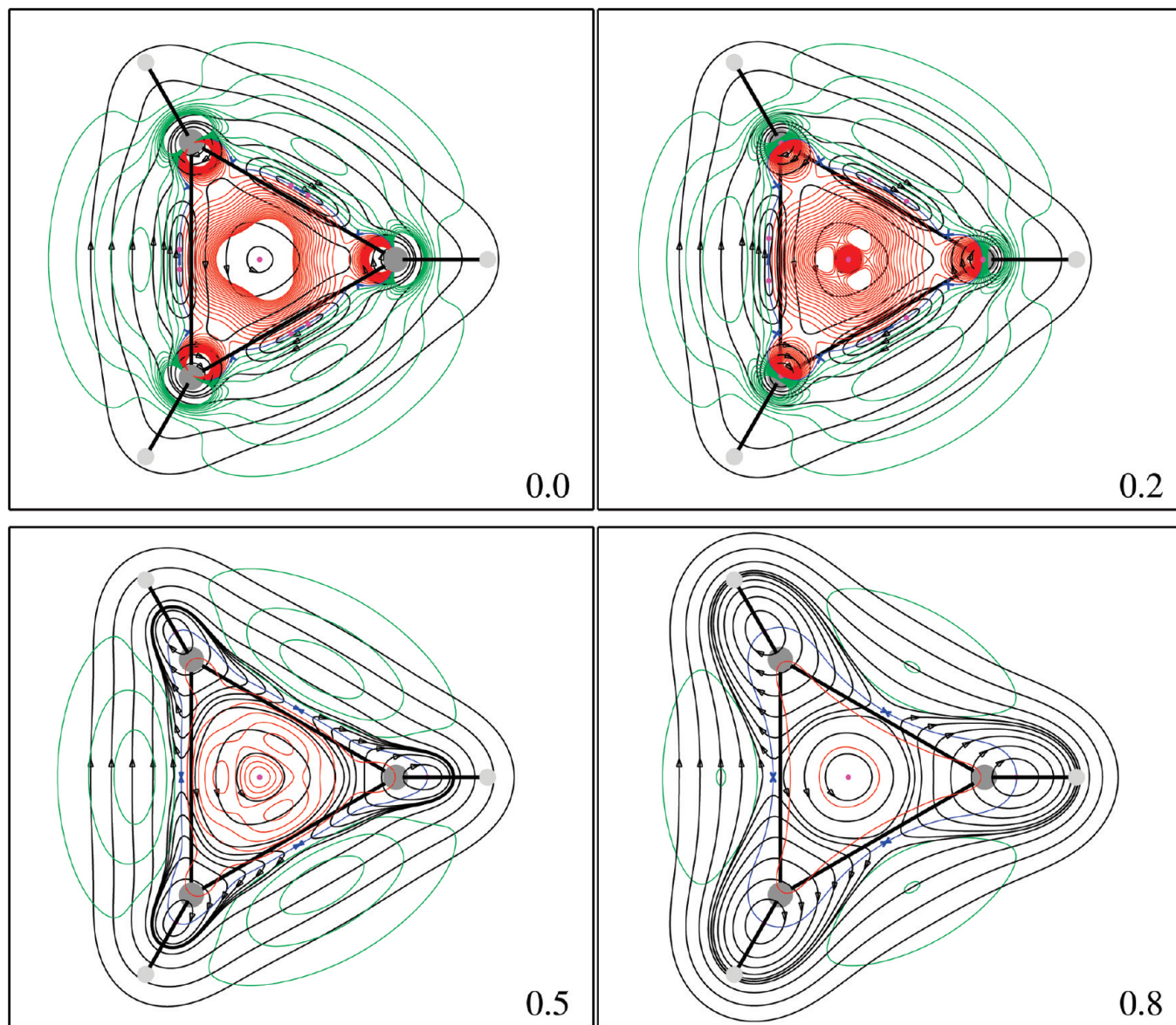


**Figure 13.** Streamlines and corresponding contours of the magnetic shielding density  $\Sigma'_{zz}$ , in au, for an applied field of 1 au, of a ghost nucleus  $l$  at the center of mass, on the plane of carbon nuclei and on three planes at distance (in bohr) 0.2, 0.5, and 0.8. The color code is the same as in Figure 11. The contributions to  $\sigma'_{zz}$  arising from the vortices flowing around the C–H bonds decrease on increasing the distance from  $\sigma_h$ . The intensity of delocalized currents beyond the methylene groups analogously decreases. On higher planes, small contributions to  $\sigma'_{zz}$  only arise from delocalized flow outside of  $\text{CH}_2\text{—CH}_2$  moieties. Truncated min, max, and step = −0.20, 0.10, and 0.010 au.

the same magnitude as that observed for  $B_{||}$  applied in the  $C_3$  direction.

Our ring current models have been compared with others previously reported,<sup>19,26</sup> displaying current flow only in the plane of the carbon nuclei, and they have been tested by checking their ability to rationalize measurable quantities, such as the components of magnetic susceptibility and shielding of hydrogen and carbon nuclei. The magnetic shielding of a probe at the center of mass has also been interpreted. The main conclusions, confirming and widening those of a previous paper,<sup>24</sup> are:

- (1) In the presence of a magnetic field  $\mathbf{B}$  perpendicular to the plane of the carbon nuclei, the induced  $\mathbf{J}^B$  field contains four whirlpools extending for more than 10 bohr, above and below the  $\sigma_h$  plane, as shown in Figure 1. The central vortex, rotating about the  $C_3$  axis,

is paratropic and of weaker intensity in comparison with the three strong diatropic vortices sustained by the  $\text{sp}^3$  hybrid carbon orbitals forming the C–H bonds. This set of vortices is enclosed within a large domain of torus-shaped diatropic flow, delocalized around the whole skeleton of C and H nuclei. Comparatively higher intensities of this delocalized flow are observed along an annulus of “ring currents” originating in the C–C bent bonds, flowing outside of the carbon nuclei and splitting into two streams along the C–H bonds.

- (2) The  $\mathbf{J}^B$  field of  $C_n\text{H}_n$  cyclic planar systems sustaining delocalized diatropic  $\pi$ -currents contains  $n$  diatropic vortices originating at two points on  $C_n$ , equally spaced with respect to the center of mass (at  $\approx \pm 2.5$  bohr in benzene)<sup>48</sup> and passing through the C–C bonds. At variance with this typical pattern, saddle regime is

- observed about the midpoint of C–C bonds in cyclopropane. Spiralling trajectories connect a set of 18 foci and 6 saddle nodes.
- (3) The near Hartree–Fock average shielding  $\sigma_{\text{av}}^{\text{H}} = 32.1$  is dominated by  $\sigma_{zz}^{\text{H}} = 37.0$  ppm. The other calculated components are  $\sigma_{xx}^{\text{H}} = 33.3$  and  $\sigma_{yy}^{\text{H}} = 26.1$  ppm. The annular flow on the  $\sigma_h$  plane, involving cyclic  $\sigma$ -electron delocalization among the three carbon atoms, referred to as a ring current by Dale Poulter et al.,<sup>7</sup> provides minor contributions to the high-field chemical shift  $\delta^{\text{H}} = \sigma_{\text{av}}^{\text{H}}(\text{TMS}) - \sigma_{\text{av}}^{\text{H}}$  from tetramethylsilane (TMS). In fact, the proton shielding is determined to comparable extent by the delocalized currents and the local vortices about the CH bonds. As the major contribution of the delocalized current to  $\sigma_{zz}^{\text{H}}$  comes from electron flow on planes close to the H nucleus, a simplified RCM should more properly consider a current loop on the plane of the hydrogen nuclei, rather than a circuit around the carbon nuclei on the  $\sigma_h$  plane.
  - (4) The local diatropic vortices sustained by the  $\text{sp}^3$  hybrid orbital cause also a major diamagnetic shift of the out-of-plane component  $\sigma_{zz}^{\text{C}} = 236.0$  ppm of the carbon shielding, a corresponding increase of the average  $\sigma_{\text{av}}^{\text{C}} = 198.1$  ppm and a sizable anisotropy  $\Delta\sigma^{\text{C}} = \sigma_{zz}^{\text{C}} - (\sigma_{xx}^{\text{C}} + \sigma_{yy}^{\text{C}})/2 = -56.9$  ppm.
  - (5) A magnetic field  $B_{\perp}$  parallel to a two-fold symmetry axis induces strong delocalized currents circulating about the entire molecule, sustained by the local charge distribution (the  $\sigma$ -electrons of the C–C “banana bond” and of the C–H bonds), as shown in Figure 6. The current susceptibility of the  $T\sigma_v \equiv xz$  half-plane, for a magnetic field in the  $C_2 \equiv x$  direction, is 15.7 nA/T, see Figure 10, that is,  $\approx 1.5$  times higher than that calculated for  $B_{\parallel}$ .
  - (6) The noncanonical “ring current without a carbon ring” circulating about the  $C_2$  axis enhances the  $\sigma_{\perp}^{\text{CM}}$  in-plane component of the shielding tensor of a probe placed in the center of mass. The near Hartree–Fock value of  $\sigma_{\perp}^{\text{CM}}$  is 50.9 ppm, that is  $\approx 18$  ppm bigger than out-of-plane  $\sigma_{\parallel}^{\text{CM}} = 32.7$  (which would be the relevant quantity for an assessment of  $\sigma$ -diamagnetic properties), thus providing a dominant contribution to the average  $\sigma_{\text{av}}^{\text{CM}} = (\sigma_{\parallel}^{\text{CM}} + 2\sigma_{\perp}^{\text{CM}})/3 = 44.9$  ppm. Therefore, neither the average NICS, defined as  $-\sigma_{\text{av}}^{\text{CM}}$ <sup>13</sup> nor  $\text{NICS}_{\parallel} = -\sigma_{\parallel}^{\text{CM}}$ <sup>66,67</sup> are reliable quantifiers of  $\sigma$ -diamagnetic properties for cyclopropane. Furthermore, if  $\sigma_{\parallel}^{\text{CM}}$  were preferred as an appropriate measure of magnetic aromaticity, one should admit that the cyclopropane molecule is even more diatropic when exposed to a magnetic field directed like a  $C_2$  symmetry axis.
  - (7) Whereas  $\sigma_{\perp}^{\text{CM}} > \sigma_{\parallel}^{\text{CM}}$ ,  $\chi_{\perp} < \chi_{\parallel}$  in cyclopropane. The peculiarity of these results, seemingly in contrast with one another, is understood by means of our RCM, recalling that the element of induced magnetic field at the position of a probe depends on the second inverse power of its distance from an element of current. The in-plane component of the shielding at the center of mass is mainly biased by the strong diatropic ring current nearest to it displayed in Figure

6. For instance, the plot of the isoshielding surface of  $\Sigma'_{\text{xx}}$  with value 0.05 in Figure 8, for a ghost atom at the midpoint of a C–C bond, shows shape and size of the shielding basin which provides big contributions to  $\sigma_{\perp}^{\text{I}}$ . The out-of-plane component  $\chi_{\parallel}$  of the magnetic susceptibility, a quantity depending on the intensity of the ring currents and on the area enclosed in the ring-current loop,<sup>63</sup> samples the whole molecular domain. As such, it can generally be considered as a more reliable measure of global diatropicity.

These results show that the basic motif of the well-established ad hoc model first proposed by Dewar<sup>15</sup> to explain chemical shifts of proton magnetic resonance is to some extent confirmed and completed by that proposed in this work. The statement that cyclopropane is an archetypal  $\sigma$ -aromatic system only on the basis of the isotropic NICS value has been demonstrated to be unsatisfactory, as much of the NICS arises from the delocalized current flowing around the  $C_2$  axes. Such a current is consistent with a significant nonlocal contribution to  $\Delta\chi$ , and it is useful to explain the surprising results reported by Benson and Flygare,<sup>5,23</sup> cited in Section 1, as well as the conflicting conclusions on relative amounts of delocalization arrived at by considering either  $\chi_{\text{av}}$  or  $\Delta\chi$ .

In fact, in Section 1, we evaluated the nonlocal contributions to  $\chi_{\text{av}}$  and  $\Delta\chi$ , that is,  $\chi_{\parallel}^{\text{nonloc}} = -14.5$  and  $\chi_{\perp}^{\text{nonloc}} = +1.9$  ppm erg G<sup>-2</sup> mol<sup>-1</sup>, respectively. The estimated positive nonlocal contribution to  $\chi_{\perp}$  depends on the assumption of  $\text{sp}^3$  hybridization of carbon valence orbitals.

On the other hand, if one accepts the Walsh idea that cyclopropane might be portrayed as a  $\pi$ -complex of one ethylene and one methylene fragments,<sup>74,75</sup> assuming  $\text{sp}^2$  hybridization, using the atomic Pascal terms  $\chi_{\text{C}} = -6.00$ ,  $\chi_{\text{H}} = -2.93$ , the correction 5.5 erg G<sup>-2</sup> mol<sup>-1</sup> for a C=C bond reported by Bain and Berry,<sup>21</sup> and the anisotropy  $\Delta\chi = 4.4 \pm 0.4$  for an  $\text{sp}^2$  carbon from Benson and Flygare,<sup>22</sup> the nonlocal contribution to the average susceptibility becomes  $\chi_{\text{av}}^{\text{nonloc}} = -39.2 - 3 \times (-6.00) - 6 \times (-2.93) - 5.5 = -9.1$ , that to the anisotropy is  $\Delta\chi^{\text{nonloc}} = -11.6 - 3 \times 4.4 = -24.8$ , so that  $\chi_{\parallel}^{\text{nonloc}} = -25.7$  and  $\chi_{\perp}^{\text{nonloc}} = -0.9$  ppm erg G<sup>-2</sup> mol<sup>-1</sup>.

Therefore, the nonlocal contribution to  $\chi_{\perp}$  becomes negative and smaller than the sum of the experimental errors. The fact that Pascal's constants are able to account for the effects of a delocalized current in cyclopropane, as well as in ethylene, is analogous to what happens in conjugated noncyclic hydrocarbons, where the stabilization energies can be obtained in terms of additive terms.<sup>76</sup>

This finding might imply that a description in terms of  $\text{sp}^2$ , instead of  $\text{sp}^3$ , carbon hybrids<sup>74,75</sup> would be preferable, which seems, to some extent, consistent with the model of the current density reported in Figures 1 and 6. In particular, the intense electron flow about a  $C_2$  symmetry axis is fully compatible with the Walsh model of cyclopropane as a  $\pi$ -complex of one ethylene moiety and one methylene fragment.<sup>74,75</sup>

**Acknowledgment.** R.C. thanks the Fund for Scientific Research (F.R.S.-FNRS) for his Research Fellow position. This work has been supported by the Belgian Government

(IUAP N P06-27 Functional Supramolecular Systems) and by a scientific collaboration between Wallonie-Bruxelles International, the FNRS, and the Italian Department of International Affairs. Financial support from the Fondazione Cassa di Risparmio di Modena and from the Italian MIUR (Ministero dell'Istruzione, dell'Università e della Ricerca) via FARB funds of the University of Salerno is gratefully acknowledged.

**Supporting Information Available:** BK and FBL ring current model. Nuclear magnetic shielding of carbon and hydrogen from the CTOCD/6-31G\*\* calculation. Magnetic susceptibilities from the CTOCD/6-31G\*\* calculation. This material is available free of charge via the Internet at <http://pubs.acs.org>.

## References

- (1) Lacher, J. R.; Pollock, J. W.; Park, J. D. *J. Chem. Phys.* **1952**, *20*, 1047–1048.
- (2) Wiberg, K.; Nist, B. *J. Am. Chem. Soc.* **1961**, *83*, 1226–1230.
- (3) Patel, D. J.; Howden, M. H.; Roberts, J. D. *J. Am. Chem. Soc.* **1963**, *85*, 3218–3223.
- (4) Burke, J. J.; Lauterbur, P. C. *J. Am. Chem. Soc.* **1964**, *86*, 1870–1871.
- (5) Benson, R. C.; Flygare, W. H. *J. Chem. Phys.* **1969**, *51*, 3087–3096.
- (6) Bley, W.-R. *Mol. Phys.* **1971**, *20*, 491–501.
- (7) Dale Poulter, C.; Boikess, R. S.; Brauman, J. I.; Winstein, S. *J. Am. Chem. Soc.* **1972**, *94*, 2291–2296.
- (8) Hahn, R. C.; Howard, P. C. *J. Am. Chem. Soc.* **1972**, *94*, 3143–3148.
- (9) Aldrich, P. D.; Kuklich, S. G.; Campbell, E. J.; Read, W. G. *J. Am. Chem. Soc.* **1983**, *105*, 5569–5576.
- (10) Lukins, P. B.; Laver, D. R.; Buckingham, A. D.; Ritchie, G. L. D. *J. Phys. Chem.* **1985**, *89*, 1309–1312.
- (11) Jiao, H.; Nagelkerke, R.; Kurtz, H. A.; Williams, R. V.; Borden, W. T.; von Ragué Schleyer, P. *J. Am. Chem. Soc.* **1997**, *119*, 5921–5929.
- (12) Flygare, W. H. *Chem. Rev.* **1974**, *74*, 653–687.
- (13) von Ragué Schleyer, P.; Maerker, C.; Dransfeld, A.; Jiao, H.; van Eikema Hommes, N. J. R. *J. Am. Chem. Soc.* **1996**, *118*, 6317–6318.
- (14) Jensen, M. Ø.; Hansen, A. E. *Adv. Quantum Chem.* **1999**, *35*, 193–215.
- (15) Dewar, M. J. S. *J. Am. Chem. Soc.* **1984**, *106*, 669–682.
- (16) Tori, K.; Kitahonoki, K. *J. Am. Chem. Soc.* **1965**, *87*, 386–387.
- (17) Forsen, S.; Norin, T. *Tetrahedron Lett.* **1964**, *5*, 2845–2849.
- (18) Graham, J. D.; Rogers, M. T. *J. Am. Chem. Soc.* **1962**, *84*, 2249–2252.
- (19) Fowler, P. W.; Baker, J.; Lillington, M. *Theor. Chem. Acc.* **2007**, *118*, 123–127.
- (20) Wu, W.; Ma, B.; Wu, J. I.-C.; von Ragué Schleyer, P.; Mo, Y. *Chem.—Eur. J.* **2009**, *15*, 9730–9736.
- (21) Bain, G. A.; Berry, J. F. *J. Chem. Educ.* **2008**, *85*, 532–536.
- (22) Benson, R. C.; Flygare, W. H. *J. Chem. Phys.* **1973**, *58*, 2366–2372.
- (23) Benson, R. C.; Flygare, W. H. *J. Chem. Phys.* **1973**, *58*, 2651–2652.
- (24) Pelloni, S.; Lazzeretti, P.; Zanasi, R. *J. Phys. Chem. A* **2007**, *111*, 8163–8169.
- (25) Lazzeretti, P.; Zanasi, R. *J. Am. Chem. Soc.* **1983**, *105*, 12–15.
- (26) Bader, R. F. W.; Keith, T. A. *J. Chem. Phys.* **1993**, *99*, 3683–3693.
- (27) Fliegl, H.; Sundholm, D.; Taubert, S.; Jusélius, J.; Klopper, W. *J. Phys. Chem. A* **2009**, *113*, 8668–8676.
- (28) Exner, K.; von Ragué Schleyer, P. *J. Phys. Chem. A* **2001**, *105*, 3407–3416.
- (29) Moran, D.; Manoharan, M.; Heine, T.; von Ragué Schleyer, P. *Org. Lett.* **2003**, *5*, 23–26.
- (30) Dewar, M. J. S.; McKee, M. L. *Pure Appl. Chem.* **1980**, *52*, 1431–1441.
- (31) Minkin, V. I.; Glukhovtsev, M. N.; Simkin, B. Y. *J. Mol. Struct. (THEOCHEM)* **1988**, *181*, 93–110.
- (32) Li, Z.-H.; Moran, D.; Fan, K.-N.; von Ragué Schleyer, P. *J. Phys. Chem. A* **2005**, *109*, 3711–3716.
- (33) Monaco, G.; Zanasi, R.; Pelloni, S.; Lazzeretti, P., in preparation.
- (34) Bettinger, H. F.; Pak, C. H.; Xie, Y. M.; von Ragué Schleyer, P.; Schaefer, H. F. *J. Chem. Soc. Perkin Trans. 2* **1999**, 2377–2381.
- (35) Sauers, R. R. *Tetrahedron* **1998**, *54*, 337–348.
- (36) Reyn, J. W. *Z. Angew. Math. Physik* **1964**, *15*, 540–557.
- (37) Lazzeretti, P. Ring Currents. In *Progress in Nuclear Magnetic Resonance Spectroscopy*; Eds: Emsley, J. W., Feeney, J., Sutcliffe, L. H. Elsevier: 2000; Vol. 36, pp 1–88.
- (38) Gomes, J. A. N. F. *J. Chem. Phys.* **1983**, *78*, 4585–4591.
- (39) Gomes, J. A. N. F. *Phys. Rev. A* **1983**, *28*, 559–566.
- (40) Gomes, J. A. N. F. *J. Mol. Struct. (THEOCHEM)* **1983**, *93*, 111–127.
- (41) Keith, T. A.; Bader, R. F. W. *J. Chem. Phys.* **1993**, *99*, 3669–3682.
- (42) Collard, K.; Hall, G. G. *Int. J. Quantum Chem.* **1977**, *XII*, 623–637.
- (43) Bader, R. F. W. *Atoms in Molecules—A Quantum Theory*; Oxford University Press: Oxford, U.K., 1990.
- (44) Milnor, J. W. *Topology from the Differentiable Viewpoint*; University of Virginia Press: Charlottesville, VA, 1997.
- (45) Guillemin, V.; Pollack, A. *Differential Topology*; Prentice-Hall: Englewood Cliffs, NJ, 1974.
- (46) The topological index  $\iota$  counts the number of times that the current density vector  $\mathbf{J}^B$  rotates completely, while one walks counterclockwise around a circle of radius  $\epsilon$  so small that  $\mathbf{J}^B$  has no zeroes inside except the SP at its center. The topological index  $\iota$  of a saddle (vortex) line is  $-1$  ( $+1$ ). Both SPs have  $(r, s) = (2, 0)$ .
- (47) Keith, T. A.; Bader, R. F. W. *Chem. Phys. Lett.* **1993**, *210*, 223–231.
- (48) Pelloni, S.; Faglioni, F.; Zanasi, R.; Lazzeretti, P. *Phys. Rev. A: At., Mol., Opt. Phys.* **2006**, *74*, 012506.

- (49) Pelloni, S.; Lazzeretti, P. *J. Chem. Phys.* **2008**, *128*, 194305-1–194305-10.
- (50) Keith, T. A.; Bader, R. F. W. *Can. J. Chem.* **1996**, *74*, 185–200.
- (51) Bader, R. F. W.; Keith, T. A. *Int. J. Quantum Chem.* **1996**, *60*, 373–379.
- (52) Pelloni, S.; Lazzeretti, P. *Theor. Chem. Acc.* **2007**, *117*, 903–913.
- (53) Pelloni, S.; Lazzeretti, P.; Zanasi, R. *J. Phys. Chem. A* **2007**, *111*, 3110–3123.
- (54) Gomes, J. A. N. F.; Mallion, R. B. *Chem. Rev.* **2001**, *101*, 1349–1383.
- (55) For detailed inspection, a graphic software is delivered, which can be used to rotate and to blow up this figure in three-dimensional space. The LINUX and WINDOWS versions of the graphic code used to obtain three-dimensional representations of the stagnation graph and current density vector field of a series of molecules can be downloaded at <https://theochem.chimfar.unimo.it/VEDO3/>.
- (56) Soncini, A.; Lazzeretti, P.; Zanasi, R. *Chem. Phys. Lett.* **2006**, *421*, 21.
- (57) Monaco, G.; Zanasi, R. *J. Chem. Phys.* **2009**, *131*, 044126.
- (58) Mitchell, R. H. *Chem. Rev.* **2001**, *101*, 1301–1315.
- (59) Hirschfelder, J. O. *J. Chem. Phys.* **1978**, *68*, 5151–5162.
- (60) Lazzeretti, P.; Malagoli, M.; Zanasi, R. *Chem. Phys. Lett.* **1994**, *220*, 299–304.
- (61) Jameson, C. J.; Buckingham, A. D. *J. Phys. Chem.* **1979**, *83*, 3366–3371.
- (62) Jameson, C. J.; Buckingham, A. D. *J. Chem. Phys.* **1980**, *73*, 5684–5692.
- (63) Since  $\mathbf{J} = \rho\mathbf{v}$ ,  $\mathbf{v} = d\mathbf{r}/dt$ ,  $\rho d^3r = dq$ , and  $i = dq/dt$ , the integrand in eq 2 is proportional to the current  $i$  and to the area element  $\epsilon_{\alpha\beta\gamma}r_\gamma dr_\beta$ .
- (64) Lazzeretti, P.; Malagoli, M.; Zanasi, R. *Project Sistemi Informatici e Calcolo Parallelo*; Research Report 1/67; Consiglio Nazionale delle Ricerche (CNR): Rome, Italy, 1991.
- (65) Coriani, S.; Lazzeretti, P.; Malagoli, M.; Zanasi, R. *Theor. Chim. Acta* **1994**, *89*, 181–192.
- (66) Lazzeretti, P. *Phys. Chem. Chem. Phys.* **2004**, *6*, 217–223.
- (67) Corminboeuf, C.; Heine, T.; Seifert, G.; von Raguer Schleyer, P.; Weber, J. *Phys. Chem. Chem. Phys.* **2004**, *6*, 273–276.
- (68) Coulson, C. A.; Moffitt, W. E. *J. Chem. Phys.* **1947**, *15*, 151.
- (69) Pelloni, S.; Lazzeretti, P. *Chem. Phys.* **2009**, *356*, 153–163.
- (70) Monaco, G.; Zanasi, R. *AIP Conf. Proc.* **2009**, *1148*, 425–428.
- (71) Lin, Y.-C.; Sundholm, D.; Jusélius, J. *J. Chem. Theory Comput.* **2006**, *2*, 761–764.
- (72) Jusélius, J.; Sundholm, D.; Gauss, J. *J. Chem. Phys.* **2004**, *121*, 3952–3963.
- (73) Farnum, D. G.; Wilcox, C. F. *J. Am. Chem. Soc.* **1967**, *89*, 5379–5383.
- (74) Walsh, A. D. *Nature* **1947**, *159*, 165.
- (75) Walsh, A. D. *Nature* **1947**, *159*, 712–713.
- (76) Dewar, M. J. S.; Llano, C. D. *J. Am. Chem. Soc.* **1969**, *91*, 789–795.

CT100175J